This article was downloaded by: [Ondokuz Mayis Universitesine]
On: 13 November 2014, At: 17:04
Publisher: Taylor & Francis
Informa Ltd Registered in England and Wales Registered Number: 1072954 Registered office: Mortimer House, 37-41 Mortimer Street, London W1T 3JH, UK

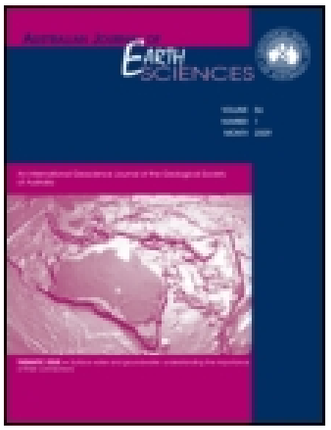

Australian Journal of Earth Sciences: An International Geoscience Journal of the Geological Society of Australia
Publication details, including instructions for authors and subscription information:
http://www.tandfonline.com/loi/taje20

Shoshonitic magmatism and the formation of the Northparkes porphyry Cu - Au deposits, New South Wales

V. Lickfold [a] , D. R. Cooke [a] , A. J. Crawford [a] & C. M. Fanning [b]

[a] ARC Centre of Excellence in Ore Deposits, University of Tasmania , Private Bag 79, Hobart, Tas., 7001, Australia

[b] PRISE, Australian National University , Canberra, ACT, 0200, Australia

Published online: 06 Oct 2011.

To cite this article: V. Lickfold , D. R. Cooke , A. J. Crawford & C. M. Fanning (2007) Shoshonitic magmatism and the formation of the Northparkes porphyry Cu - Au deposits, New South Wales, Australian Journal of Earth Sciences: An International Geoscience Journal of the Geological Society of Australia, 54:2-3, 417-444, DOI: 10.1080/08120090601175754

To link to this article: http://dx.doi.org/10.1080/08120090601175754

PLEASE SCROLL DOWN FOR ARTICLE

Taylor & Francis makes every effort to ensure the accuracy of all the information (the "Content") contained in the publications on our platform. However, Taylor & Francis, our agents, and our licensors make no representations or warranties whatsoever as to the accuracy, completeness, or suitability for any purpose of the Content. Any opinions and views expressed in this publication are the opinions and views of the authors, and are not the views of or endorsed by Taylor & Francis. The accuracy of the Content should not be relied upon and should be independently verified with primary sources of information. Taylor and Francis shall not be liable for any losses, actions, claims, proceedings, demands, costs, expenses, damages, and other liabilities whatsoever or howsoever caused arising directly or indirectly in connection with, in relation to or arising out of the use of the Content.

This article may be used for research, teaching, and private study purposes. Any substantial or systematic reproduction, redistribution, reselling, loan, sub-licensing, systematic supply, or distribution in any form to anyone is expressly forbidden. Terms & Conditions of access and use can be found at http://www.tandfonline.com/page/terms-and-conditions

Australian Journal of Earth Sciences (2007) **54**, (417–444)

Shoshonitic magmatism and the formation of the Northparkes porphyry Cu–Au deposits, New South Wales

V. LICKFOLD[1]*, D. R. COOKE[1†], A. J. CRAWFORD[1] AND C. M. FANNING[2]

[1]*ARC Centre of Excellence in Ore Deposits, University of Tasmania, Private Bag 79, Hobart, Tas. 7001, Australia.*
[2]*PRISE, Australian National University, Canberra, ACT 0200, Australia.*

Four economic porphyry Cu–Au deposits occur at Northparkes, New South Wales: Endeavour 22 (E22), E26, E27 and E48. Mineralisation is centred on thin, pipe-like Late Ordovician to Early Silurian quartz monzonite porphyry complexes. Nine intrusive phases have been recognised, with a common sequence of emplacement recognised in all deposits. Pre-mineralisation intrusions include coarse-grained, equigranular monzodiorite and equigranular to weakly porphyritic biotite–quartz monzonite (U–Pb SHRIMP age 444.2 ± 4.7 Ma). Three variably felsic quartz monzonite porphyry phases comprise the mineralised intrusive complexes: (i) volumetrically minor early and late mineralisation biotite-phyric quartz monzonite porphyry dykes; (ii) abundant synmineralisation K-feldspar-phyric quartz monzonite porphyry intrusions; and (iii) less abundant syn- to late mineralisation augite–biotite K-feldspar-phyric quartz monzonite porphyry intrusions. Post-mineralisation basaltic trachyandesite dykes and augite-phyric monzonite porphyry dykes are also present (U–Pb SHRIMP age 436.7 ± 3.3 Ma), as are younger mafic dykes. The regional volcanic and intrusive rocks define systematic geochemical trends consistent with high-temperature magmatic fractionation of basaltic trachyandesite through trachyte. However, the trace-element compositions and REE patterns of the mineralising intrusions cannot be explained by crystal fractionation alone because there is a return to more mafic compositions in the waning stages of intrusive activity. The intrusive complexes are interpreted to have formed due to the emplacement of mafic alkaline melts into the base of a crystallising, zoned, monzodiorite to monzonite magma chamber. Shallow crustal fault ruptures above the magma chamber probably caused instantaneous depressurisation and simultaneous egress of quartz monzonite porphyry and exsolved aqueous fluid into dilatant zones. Localised fracturing and additional volatile exsolution from the quartz monzonite melt is thought to have led to the formation of the quartz monzonite porphyry complexes and associated Cu–Au-bearing stockwork veins and related orthoclase alteration. Volatile-rich aqueous fluid partitioned LREE preferentially to MREE and HREE resulting in the development of distinctive U-shaped REE patterns of the ore-related intrusions.

KEY WORDS: alkalic, copper, gold, magma mingling, magmatism, Northparkes, porphyry, shoshonite.

Downloaded by [Ondokuz Mayis Universitesine] at 17:04 13 November 2014

INTRODUCTION

Most porphyry-style copper–(gold–molybdenum) deposits are centred on multiphase intrusive complexes (Gustafson & Hunt 1975; Sillitoe & Gappe 1984; Carten *et al.* 1988; MacDonald & Arnold 1994; Heithersay & Walshe 1995; Lang & Titley 1998; Proffett 2003; Wilson *et al.* 2003; Seedorff & Einaudi 2004; Cooke *et al.* 2007). High-grade ore formation is typically related to one or two phases in the intrusive complex. Late stage intrusions typically dilute or truncate grade (Sillitoe 2000).

The Northparkes district in central-western New South Wales (Figure 1) contains four alkalic porphyry Cu–Au deposits, referred to as Endeavour 22 (E22), Endeavour 26 (E26), Endeavour 27 (E27) and Endeavour 48 (E48), or collectively, the Northparkes porphyry Cu–Au deposits. They have a combined resource of 131.7 Mt @ 1.12% Cu and 0.51 g/t Au (Cooke *et al.* 2007). Mineralisation is intimately associated with quartz monzonite porphyry intrusions, which are exposed to depths of 1500 m below surface via diamond drilling, openpit and underground block cave mining. Up to six discrete intrusive phases have been recognised at each deposit. This paper documents the geochemical evolution of the intrusive complexes at Northparkes, based on the relative timing of intrusions reported by Lickfold *et al.* (2003).

Previous geochemical studies at Northparkes have generally been restricted to the quartz monzonite porphyry intrusive complexes central to each deposit (Heithersay 1991; Müller *et al.* 1994; Wolfe 1994; Blevin & Morrison 1997). Differences between mineralised and unmineralised intrusions in the region have received little attention previously. Here, we compare the

*Present address: Mineral Asset Management, Kumba Resources, PO Box 9229, Pretoria, 0001, South Africa.
†Corresponding author: d.cooke@utas.edu.au

ISSN 0812-0099 print/ISSN 1440-0952 online © 2007 Geological Society of Australia
DOI: 10.1080/08120090601175754

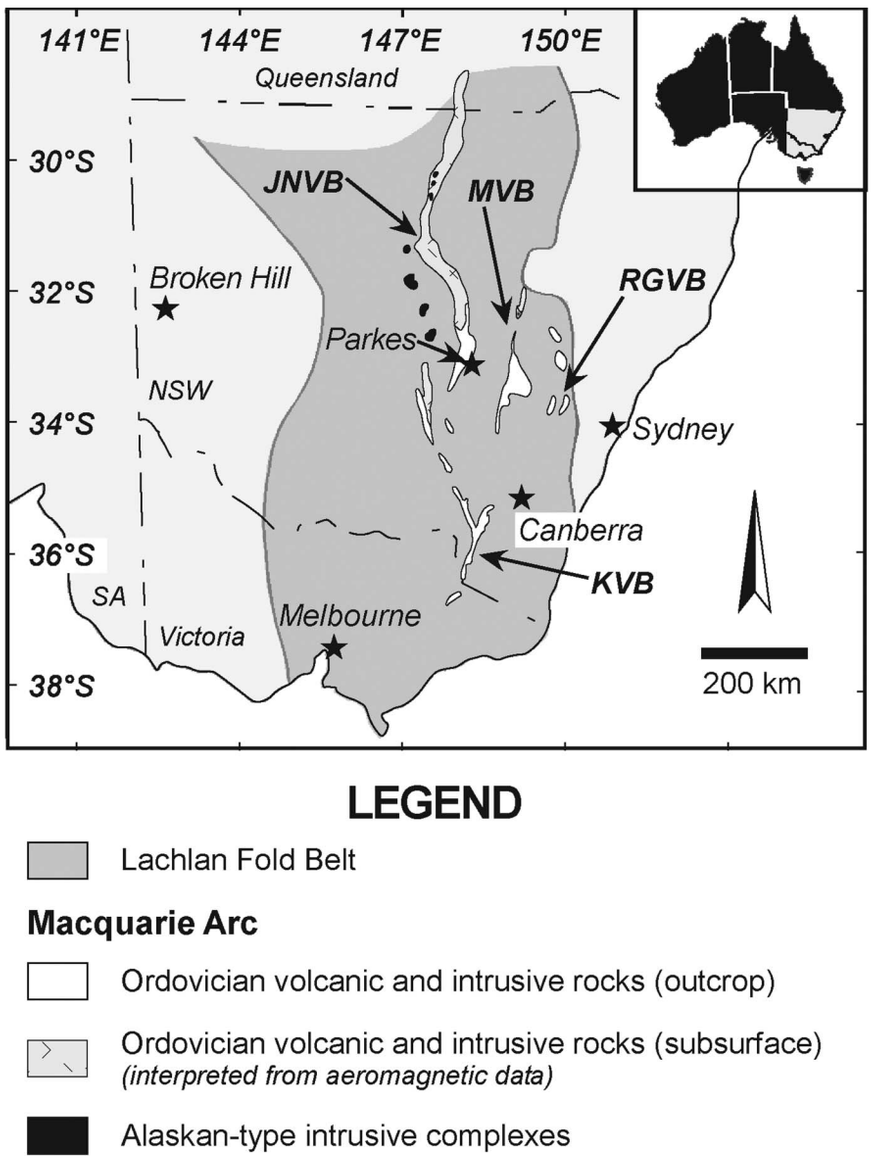

Figure 1 Distribution of Ordovician to Silurian volcanic and intrusive rocks of the Macquarie Arc, part of the Lachlan Fold Belt of central New South Wales (modified after Scheibner & Basden 1998; Lickfold *et al.* 2003). JNVB, Junee–Narromine Volcanic Belt; MVB, Molong Volcanic Belt; RGVB, Rockley–Gulgong Volcanic Belt; KVB, Kiandra Volcanic Belt.

geochemical characteristics of the mineralised intrusions at Northparkes with the unmineralised intrusive rocks in the region in order to: (i) speculate on the processes that once might have operated in the parental magma bodies to produce the Northparkes porphyry Cu–Au deposits; and (ii) determine whether any geochemical characteristics are unique to the mineralising intrusions.

Previous work

The Northparkes (formerly Goonumbla) district is situated 20–30 km northwest of Parkes in central-western New South Wales, ~300 km west of Sydney (Figures 1, 2). The first porphyry-related Cu–Au mineral occurrence in this region was discovered in 1976. Subsequent exploration led to the discovery of several Late Ordovician to Early Silurian Cu–Au porphyry deposits centred on quartz monzonite porphyry complexes at Northparkes (Figure 3). More recent discoveries of similar styles of alkalic porphyry Cu–Au deposits at Cadia (Holliday *et al.* 2002; Wilson *et al.* 2003, in press) highlight the economic significance of this mineral province.

Previous studies of the Northparkes district include Jones (1985) and Heithersay *et al.* (1990). House (1994), Heithersay and Walshe (1995) and Harris (1997) described the geology of the E26 deposit. The multiphase quartz monzonite porphyry complexes and associated alteration and vein mineralisation at E48 and E27 have been described by Wolfe (1994) and Hooper *et al.* (1996), and by Squires (1992), respectively. Lickfold (2002) and Lickfold *et al.* (2003) described the intrusive history and volatile evolution of the four major Northparkes porphyry Cu–Au deposits. A magmatic origin for phyllic alteration assemblages at E48 and E26 has been demonstrated by Wolfe *et al.* (1996) and Harris and Golding (2002), respectively. Regional geological studies include Bowman *et al.* (1982), Clarke (1990), Krynen *et al.* (1990), Hall (1993), Sherwin (1996) and Duggan *et al.* (1999). Müller *et al.* (1994) discussed the association of the Northparkes porphyry Cu–Au deposits with

Downloaded by [Ondokuz Mayis Universitesine] at 17:04 13 November 2014

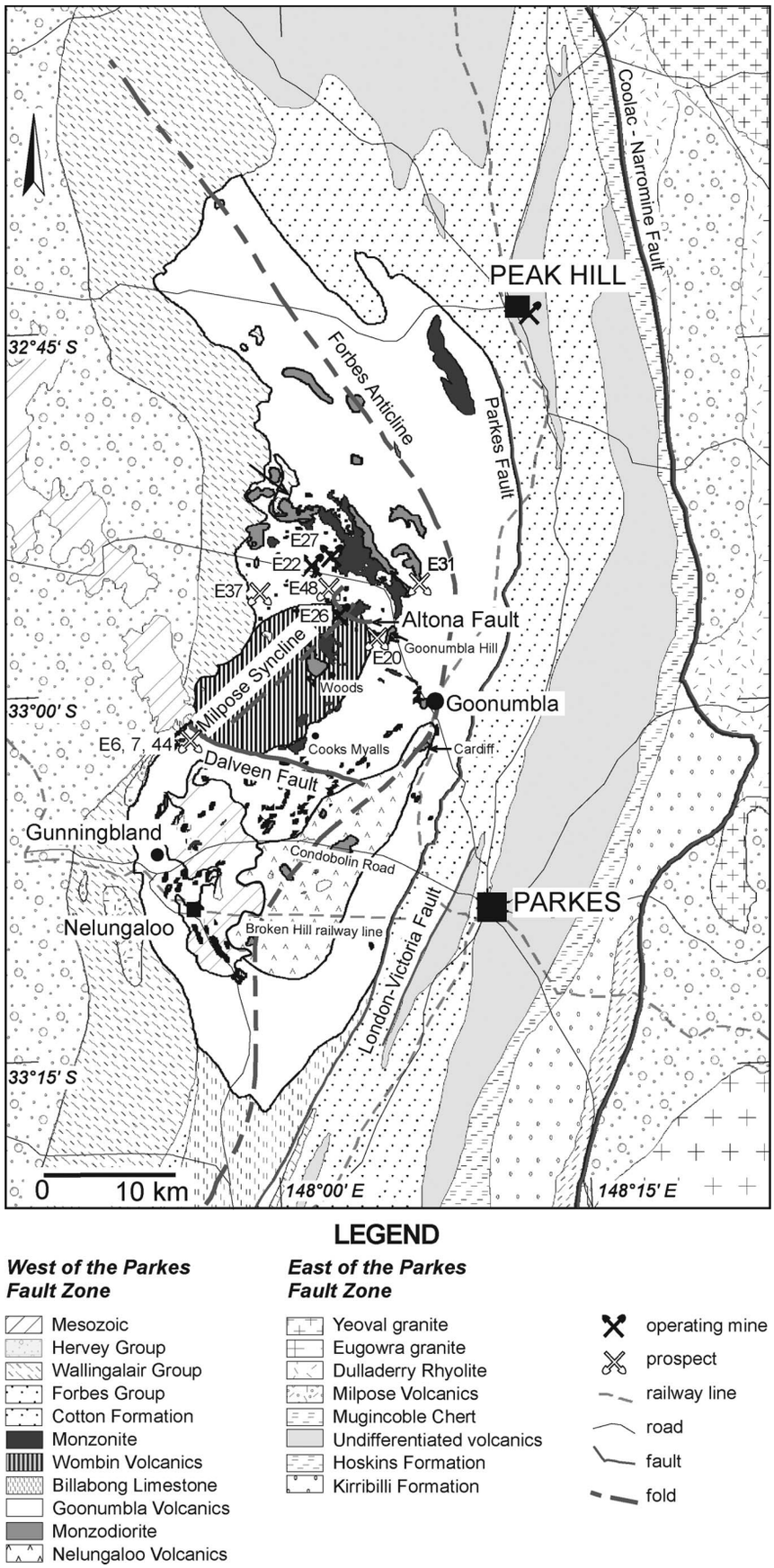

Figure 2 Local geology of the Parkes district, New South Wales (modified after Heithersay *et al.* 1990; Heithersay & Walshe 1995; Lickfold *et al.* 2003).

Downloaded by [Ondokuz Mayis Universitesine] at 17:04 13 November 2014

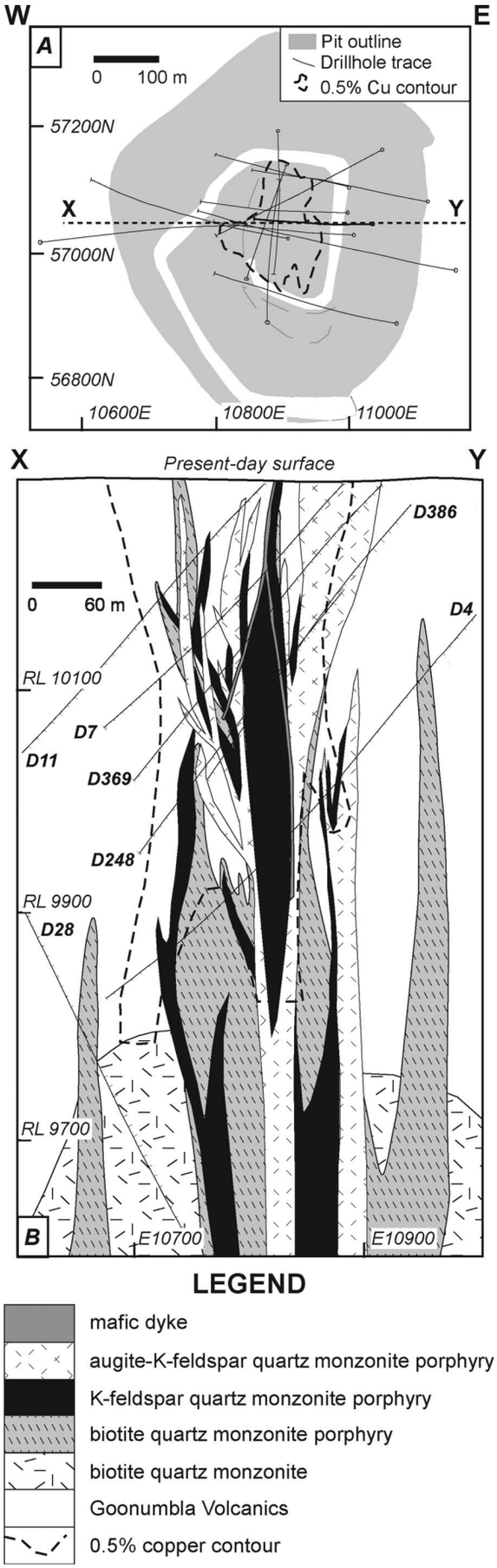

shoshonitic magmatism. Butera *et al.* (2001) reported U–Pb (SHRIMP) dating of several regional intrusions. Scott (2005) reported on the effectiveness of rutile geochemistry as an exploration vector to the Northparkes porphyry deposits. Simpson *et al.* (2005) described the district volcanology, whereas Lye *et al.* (2006) provided the most recent summary of the exploration history.

REGIONAL AND LOCAL GEOLOGY

The Northparkes deposits are hosted in the Upper Ordovician Northparkes Group (Percival & Glen 2007), part of the Ordovician to Early Silurian Junee–Narromine Volcanic Belt in the eastern Lachlan Fold Belt (Figure 1). The Junee–Narromine Volcanic Belt is one of four Ordovician volcanic belts in the region, the others being the Molong and the Rockley-Gulgong Volcanic Belts to the east, and the Kiandra Volcanic Belt to the southeast (Figure 1). These belts are inferred to represent structurally disrupted and dislocated slices of the Ordovician Macquarie island arc (Glen *et al.* 1998).

North-northeast-trending folds that have no associated axial-planar cleavage, such as the Forbes Anticline (Figure 2), are associated with conjugate east-southeast-trending dextral and north-northeast-trending sinistral brittle fault zones, such as the Dalveen Fault (Figure 2), which has a dextral offset of <2 km (Simpson *et al.* 2005). Most rocks of the Northparkes district have been metamorphosed to prehnite–pumpellyite or lower greenschist facies, with rare occurrences of zeolite facies rocks (Heithersay *et al.* 1990). Tilting or folding of the volcanic rocks occurred prior to emplacement of composite pipes of mineralised quartz monzonite porphyry intrusions. The pipes have retained a subvertical orientation since their emplacement in the Late Ordovician (Jones 1985; Arundell 1997).

The Northparkes porphyry Cu–Au deposits occur on a north-northwest-trending structural corridor that is apparent on aeromagnetic images. This structural feature is known as the Endeavour Linear (Jones 1985; Heithersay & Walshe 1995). They also occur close to the arc-transverse Lachlan Transverse Zone, a regional-scale west-northwest-trending structure that extends across much of New South Wales (Glen & Walshe 1999). Pipe-like quartz monzonite porphyry intrusions at Northparkes were emplaced at the intersection of major northwest- and northeast-trending fracture zones (Harris 1997; North Ltd 1999). Post-mineralisation deformation has produced low-angle thrusts, which have disrupted some of the porphyry deposits [e.g. E48 (Hooper *et al.* 1996); E28 (Kolkert 1998)].

Figure 3 (a) Plan and (b) interpretive east–west section (mine section 57 050N) of the quartz monzonite porphyry intrusive complex central to the Endeavour 27 deposit. Drillhole data projected up to 200 m onto section (from Lickfold 2002).

Downloaded by [Ondokuz Mayis Universitesine] at 17:04 13 November 2014

Downloaded by [Ondokuz Mayis Universitesine] at 17:04 13 November 2014

Nelungaloo Volcanics

The oldest rocks exposed in the Junee–Narromine Volcanic Belt are the Lower Ordovician Nelungaloo Volcanics (Sherwin 1996; Glen *et al.* 2007; Percival & Glen 2007). The Nelungaloo Volcanics crop out in the core of the Forbes Anticline (Figure 2) and, assuming no structural repetition, have a thickness of at least 650 m (Krynen *et al.* 1990). They comprise a sequence of coherent, mainly plagioclase + clinopyroxene + olivine + Fe–Ti oxide-phyric, high-K calc-alkaline to shoshonitic andesites and volcaniclastic sedimentary rocks (Crawford *et al.* 2007; Glen *et al.* 2007) that are overlain by volcanic conglomerate, coarse-grained volcanic sandstone and the sedimentary units of the Yarrimbah Formation. Fossils from the Yarrimbah Formation indicate an Early Ordovician age for the Nelungaloo Volcanics (Krynen *et al.* 1990; Glen *et al.* 2007).

Northparkes Group

Percival and Glen (2007) defined the Northparkes Group to include the Middle–Upper Ordovician lavas, volcaniclastic deposits, shallow-water carbonates and deeper-water clastic rocks that crop out west of the Parkes thrust. The Northparkes Group is a modification of the Northparkes Volcanic Group proposed by Percival (2000) and includes two units, the Goonumbla Volcanics and the Wombin Volcanics, which host porphyry-style mineralisation at Northparkes.

GOONUMBLA VOLCANICS

The Goonumbla Volcanics are exposed on the western limb of the Forbes Anticline and in the core of the Milpose Syncline (Figure 2). They are separated from the underlying Nelungaloo Volcanics by an interpreted low-angle unconformity (Krynen *et al.* 1990). Volcanic rocks in a narrow strip on the eastern limb of the Forbes Anticline adjacent to the Parkes Thrust (Figure 2) were previously correlated with the Goonumbla Volcanics by Percival (2000) but are now excluded from the Northparkes Group (Percival & Glen 2007). The Goonumbla Volcanics are a 2.5–4 km-thick sequence of mainly basaltic andesite to trachyandesite and associated volcaniclastic rocks (Simpson *et al.* 2005; Crawford *et al.* 2007). The basal basaltic andesite is overlain by a thick package of trachyandesite and associated volcaniclastic conglomerate. The trachyandesites are massive to autobrecciated coherent units. Some are shallow, conformable sills that were emplaced into wet sediments, based on the local occurrence of peperitic upper and lower margins (Kolkert 1998; Simpson *et al.* 2005). Darriwilian to Early Bolindian fossils have been reported from the Billabong Creek Limestone and Gunningbland Formation (Krynen *et al.* 1990; Percival & Glen 2007), indicating an upper age limit of Late Ordovician for the Goonumbla Volcanics.

WOMBIN VOLCANICS

The intermediate to felsic Wombin Volcanics are distinguished from the Goonumbla Volcanics mainly due to their distinctive reddish colour (Krynen *et al.* 1990) and more evolved chemical compositions. They crop out on both limbs of the Forbes Anticline and in the southwestern part of the Milpose Syncline (Figure 2). This 700–1000 m-thick sequence comprises typically dark-red polymictic volcanic breccia and other volcaniclastic units, with less abundant porphyritic trachyandesite, flow-banded trachyte lavas and ignimbrites (Bowman *et al.* 1982; Simpson *et al.* 2005). The Wombin Volcanics conformably overlie the Goonumbla Volcanics. Simpson *et al.* (2005) interpreted the Goonumbla and Wombin Volcanics to comprise a thick (several kilometres), subaqueous volcaniclastic apron that formed on the flanks of a shallow-marine to possibly subaerial stratovolcano during the Mid to Late Ordovician. They argued that the presence of ignimbrites and trachyte lava indicated voluminous explosive eruptions and sector collapse on a possibly subaerial part of the volcano (Simpson *et al.* 2005).

Intrusive rocks

Monzodiorite intrusions in the Nelungaloo Volcanics crop out in two areas: along the Condobolin Road ~10 km west of Parkes, and to the northeast and southwest of Nelungaloo Siding (Figure 2). These intrusions have dark-green-grey, coarse-grained and equigranular interiors, and are weakly to strongly porphyritic at their margins. They contain abundant (up to 80%) euhedral plagioclase, augite and interstitial alkali feldspar. The monzodiorite along Condobolin Road has intruded the base of the Nelungaloo Volcanics and yielded a U–Pb (SHRIMP) age of 481 ± 4 Ma (Butera *et al.* 2001; Simpson *et al.* 2005; Percival & Glen 2007) (Table 1; Figure 2), corroborating the Early Ordovician fossil ages for the Nelungaloo Volcanics.

Rocks intruding the Goonumbla Volcanics are mainly monzodioritic (Krynen *et al.* 1990) and occur at three main localities: Cardiff, Goonumbla Hill and Goonumbla (Figure 2). These monzodiorite intrusions are fine- to medium-grained (0.5–2 mm) and massive to weakly porphyritic. A monzodiorite intrusion with a U–Pb age of 450.8 ± 4.2 Ma has intruded the basal Goonumbla Volcanics near Goonumbla (Butera *et al.* 2001) (Table 1; Figure 2), constraining a Middle to Late Ordovician age for the lower Goonumbla Volcanics.

Numerous monzonite and quartz monzonite bodies have intruded the Wombin Volcanics, including the quartz monzonite porphyry complexes associated with the Northparkes deposits, and monzonite porphyries at Gunningbland (Figure 2). The age of the Wombin Volcanics is not well constrained, although samples described as 'andesite' and 'gabbro' by Krynen *et al.* (1990) yielded latest Ordovician to earliest Silurian K–Ar ages. In addition, zircon grains from two monzonite intrusions, the 'Woods' monzonite and a monzonite dyke ~3 km east of Cooks Myalls (Figure 2), have yielded U–Pb (SHRIMP) ages of 439.1 ± 4.5 Ma and 438.9 ± 4.7 Ma, respectively (Butera *et al.* 2001) (Table 1).

Mineralised intrusive complexes

The quartz monzonite porphyry complexes central to the Northparkes deposits are vertically elongated,

Table 1 Geochronology of intrusive rocks from the Northparkes district.

Sample	Mineral	Method	Age (Ma)	Reference
Monzodiorite E26 (E26/46/1720.2 m)	Hornblende (p)	$^{40}Ar/^{39}Ar$	495.6 ± 26.4[a]	Lickfold *et al.* (2003)
BQM, E26 (E26/284/318.0 m)	Biotite (p)	$^{40}Ar/^{39}Ar$	437.3 ± 2.1[b]	Lickfold *et al.* (2003)
Pre-mineral B-QMP, E22 (E22/39/581.0 m)	Biotite (p)	$^{40}Ar/^{39}Ar$	448.6 ± 7.0[c]	Lickfold *et al.* (2003)
Late-mineral B-QMP, E26 (E26/46/1161.6 m)	Biotite (p)	$^{40}Ar/^{39}Ar$	446.5 ± 2.6[a]	Lickfold *et al.* (2003)
Alteration/mineralisation, E26 (E26/286/153.9 m)	Biotite (s)	$^{40}Ar/^{39}Ar$	441.3 ± 3.8[d]	Lickfold *et al.* (2003)
Alteration/mineralization, E26	Sericite	$^{40}Ar/^{39}Ar$	439.2 ± 1.2	Perkins *et al.* (1990)
Wombin intrusion[e]	Zircon	U–Pb (SHRIMP)	438.5 ± 3.6	Perkins *et al.* (1990)
Condobolin monzodiorite	Zircon	U–Pb (SHRIMP)	481 ± 4	Butera *et al.* (2001); recalculated by I. Campbell *in* Simpson *et al.* (2005)
Goonumbla monzodiorite	Zircon	U–Pb (SHRIMP)	450.8 ± 4.2	Butera *et al.* (2001)
Wombin intrusion	Zircon	U–Pb (SHRIMP)	438.9 ± 4.7	Butera *et al.* (2001)
Wombin intrusion	Zircon	U–Pb (SHRIMP)	439.1 ± 4.5	Butera *et al.* (2001)
E37 zero porphyry	Zircon	U–Pb (SHRIMP)	436.7 ± 3.3	This study
BQM, E26 (E26/287/220.6 m)	Zircon	U–Pb (SHRIMP)	444.2 ± 4.7	This study

p, primary phenocryst; s, secondary phase.
[a]correlation age.
[b]plateau age.
[c]integrated age.
[d]maximum age.
[e]interpreted as an intrusion into the Wombin Volcanics, not the Nelungaloo Volcanics, as Perkins *et al.* (1990) proposed.

pipe-like intrusive bodies (Figures 3, 4a, b). They are associated with mineralisation and alteration assemblages interpreted to have formed by late-stage release of magma and volatiles from a deep-seated magma chamber (Heithersay 1994; Heithersay & Walshe 1995; Blevin & Morrison 1997; Lickfold *et al.* 2003). Multiple intrusive phases have been recognised in each of the quartz monzonite porphyry complexes (Heithersay *et al.* 1990; House 1994; Wolfe 1994; Harris 1997). Lickfold *et al.* (2003) studied all four Northparkes deposits and recognised nine different rock types related to five intrusive events based on intrusive relationships and petrographic criteria. From oldest to youngest, these may be summarised as follows:

(1) Coarse-grained (2–3 mm) equigranular monzodiorite, restricted to the deeper portions of the E26 deposit.

(2) Weakly mineralised, equigranular to weakly porphyritic, brick-red biotite–quartz monzonite (BQM) stocks (Figures 3, 4c). These intrusions are abundant in the lower portions of all four deposits. Erratic, locally high Cu and Au grades occur at the margins of some of these intrusions (e.g. the E31 stock: Arundell 1998).

(3) Quartz monzonite porphyry dykes and pipe-like intrusions that have intruded the BQM, starting with (3a) minor volume, early-mineralisation biotite quartz monzonite porphyry (B-QMP) dykes that are preserved on the peripheries of the intrusive complexes. These were followed by: (3b) Voluminous synmineralisation K-feldspar-phyric quartz monzonite porphyry (K-QMP) dykes and pipe-like intrusions (described as 'QMP-1' by Heithersay & Walshe 1995) (Figure 4d), which typically occur in the centres of the deposits. Unidirectional solidification textures, or comb-quartz layers (Kirkham & Sinclair 1988) (Figure 4e), and miarolitic cavities have been recognised in the K-QMP intrusions from all four Northparkes deposits (Lickfold *et al.* 2003). Hydrothermal alteration zones and the highest grade ore at each deposit are centred on and most intensely developed within the K-QMP intrusions and in the immediately adjacent volcanic rocks. (3c) Late-mineralisation augite–biotite–K-feldspar quartz monzonite porphyry (KA-QMP) intrusions (Figure 4f), including a microgranite intrusion at the E48 deposit, intruded the complexes after the K-QMP pipes and dykes. KA-QMP intrusions were described as 'QMP-2' by Heithersay and Walshe (1995). They are the second-most voluminous phases in the Northparkes deposits and are associated with less intense hydrothermal alteration and lower grade Cu–Au ore than the K-QMP intrusions, and contain sulfide clots and mafic xenoliths (Figure 4b). (3d) Late-mineralisation intrusive activity culminated with the intrusion of a second phase of minor volume B-QMP dykes.

(4) Post-mineralisation intrusions, which include: (4a) basaltic trachyandesite dykes, which are intimately associated with (4b) 'zero porphyries', a local mine term for post-mineralisation, zero grade (zero Cu or Au grade), mafic monzonite porphyry dykes (Figure 4g, h) that have intruded the eastern and central parts of E26.

(5) Mafic dykes of indeterminate age. These were the youngest intrusions emplaced at Northparkes. It is possible that at least some mafic dykes were emplaced during the waning stages of Ordovician magmatism in the Northparkes district (Figure 4g). Others may be as young as Tertiary in age (Duggan *et al.* 1999).

See Lickfold *et al.* (2003) for more details concerning the mineralogy and crosscutting relationships of the intrusive rocks.

Downloaded by [Ondokuz Mayis Universitesine] at 17:04 13 November 2014

Downloaded by [Ondokuz Mayis Universitesine] at 17:04 13 November 2014

GEOCHRONOLOGY

An average $^{40}Ar/^{39}Ar$ isotopic age of 439.2 ± 1.2 Ma from white mica alteration associated with mineralisation at E26 was proposed as the age of magmatic–hydrothermal activity at Northparkes, based on its correlation with a 438.5 ± 3.6 Ma U–Pb (SHRIMP) age determination from an intrusion in the Wombin Volcanics (Perkins *et al.* 1990) (Table 1). This is consistent with the two U–Pb (SHRIMP) ages that Butera *et al.* (2001) obtained on intrusions from the Wombin Volcanics (438.9 ± 4.7 Ma, 439.1 ± 4.5 Ma: Table 1). Lickfold *et al.* (2003) reported four $^{40}Ar/^{39}Ar$ isotopic ages for primary and secondary biotite from intrusive rocks in the Northparkes district that ranged from 448.6 ± 7.0 to 437.3 ± 2.1 Ma (Table 1), consistent with a Late Ordovician to Early Silurian timing of intrusive activity in the Wombin Volcanics.

We have generated two U–Pb (SHRIMP) ages to further constrain the timing of intrusive activity at Northparkes. Analyses were conducted at the Research School of Earth Sciences, Australian National University, Canberra. The analytical method and results are given in Appendix 1. Zircons from a sample of biotite–quartz monzonite from E26 yielded a U–Pb (SHRIMP) age of 444.2 ± 4.7 Ma, which is within error of the biotite $^{40}Ar/^{39}Ar$ age of 439.0 ± 5.2 Ma from the same intrusion (Table 1). U–Pb (SHRIMP) dated zircons from a zero porphyry dyke at the Endeavour 37 (E37) copper prospect (Figure 2) yielded an age of 436.7 ± 3.3. Based on the data in Table 1, we conclude that much of the intrusive activity in the Wombin Volcanics and magmatic–hydrothermal alteration associated with the Northparkes deposits occurred at 445–437 Ma (Figure 5). However, the available ages are not precise enough to yield definitive evidence of the sequence of emplacement of individual intrusions within the quartz monzonite porphyry complexes, or to constrain the duration of discrete mineralising events.

MAJOR- AND TRACE-ELEMENT GEOCHEMISTRY

A total of 281 intrusive and volcanic rocks have been analysed for their major- and trace-element compositions by X-ray fluorescence (XRF). This includes 56 analyses from the current study (Table 2). The additional data are from Clarke (1990), Heithersay (1991), Squires (1992), Hall (1993), Müller *et al.* (1994), Wolfe (1994), Radclyffe (1995), Howland-Rose (1996), Blevin and Morrison (1997), Crawford (2001) and unpublished Northparkes Mines data.

Nelungaloo Volcanics, Northparkes Group and related intrusions

Glen *et al.* (2007) showed that the Lower Ordovician lavas and broadly comagmatic intrusive rocks of the Nelungaloo Volcanics are medium- to mainly high-K calc-alkaline andesites, basaltic andesites, and monzodiorites. The lavas and shallow intrusive sills of the Goonumbla and Wombin Volcanics and related intrusive rocks are high-K calc-alkaline to shoshonitic trachybasalts, trachyandesites, trachytes and their intrusive equivalents (Crawford *et al.* 2007). The Wombin Volcanics tend to be more felsic, with trachyandesites and trachytes containing 60–65% SiO_2 and <2% MgO. Fields defined by these units are remarkably coherent given the extended period of volcanic activity, from the Early Ordovician (Nelungaloo) to *ca* 440 Ma (Wombin Volcanics). The volcanic rock analyses show smooth MgO, TiO_2, Fe_2O_3 and CaO depletion patterns with fractionation that typifies calc-alkaline and shoshonitic suites (Figure 6). Basaltic rocks in the Goonumbla and Wombin Volcanics have the highest P_2O_5 contents (Figure 6), which then decrease with fractionation. This most likely indicates apatite saturation at the basaltic stage of magmatic evolution and indicates, by comparison with Southwest Pacific arc suites, the shoshonitic affinities of these suites. In contrast, most of the Nelungaloo rocks, at 50–53% SiO_2, have notably lower P_2O_5 contents. In these cases, apatite saturation must have occurred at ~56% SiO_2, consistent with the medium-K to high-K calc alkaline affinities of the Nelungaloo Volcanics.

In the Goonumbla Volcanics, there is a distinct increase in Al_2O_3 with decreasing MgO contents to ~2%, reflecting little, if any, removal of plagioclase during fractionation (Figure 6). For MgO <2%, there is a sharp decrease in Al_2O_3 contents for the Wombin Volcanics, reflecting significant plagioclase extraction. Despite limited Na_2O mobility during pervasive low-grade metamorphism, there is a distinct increase in Na_2O with increasing fractionation for the Goonumbla and Wombin Volcanics (Figure 6).

A notable difference between the volcanic rocks of the Nelungaloo Volcanics compared to the Goonumbla and Wombin suites is the significantly higher light rare-earth element (LREE: La, Ce, Nd) abundances in the former, despite the higher P_2O_5 and K_2O contents of the latter suites (Figure 6). This possibly reflects a source mantle feature (Crawford *et al.* 2001). In contrast, there are no consistent differences between the Nelungaloo, Goonumbla and Wombin Volcanics in terms of SiO_2 *vs* Y relationships (Figure 6). Ba and Rb show the expected general increase with increasing SiO_2, whereas Nb abundances are more variable (Figure 6). High Sr abundances (1200–1800 ppm) in many of the Goonumbla and Wombin volcanic rocks are notable.

As with other incompatible elements, Zr increases with increasing SiO_2 contents for intrusive rocks in the Goonumbla and Wombin Volcanics. However, for some intrusions in the Wombin Volcanics, there is a distinct drop in the amount of Zr increase with respect to SiO_2 for SiO_2 contents > ~58% (Figures 6, 7). This depleted-Zr trend is also evident on MgO *vs* Zr plots (Lickfold 2002), and probably reflects the onset of zircon crystallisation at ~58% SiO_2 and 3–3.5% MgO. Heithersay and Walshe (1995) recognised the depleted-Zr trend from intrusions in the Wombin Volcanics close to the Northparkes porphyry Cu–Au deposits. We have found that other intrusions associated with the Wombin Volcanics, but distal to the mineralised systems (e.g. Gunningbland monzonite porphyries), plot on an undepleted-Zr trend (Figure 6).

On multi-element plots in which rock compositions are normalised to abundances in depleted mid-ocean ridge basalts (N-MORB), arc-type magmas are typically enriched in large ion lithophile elements (LILE) such as Rb, Ba, Sr, Th and LREE relative to MORB. They also show pronounced negative Nb–Ta anomalies relative to K and La and Ce and positive Sr and Pb anomalies relative to Ce and Pr (Sun & McDonough 1989). Volcanic and intrusive rocks from the North-parkes district show spiked patterns characteristic of island arc rocks (Figure 8), with strong LILE, Pb and Sr enrichment, compared to N-MORB. In general, for the

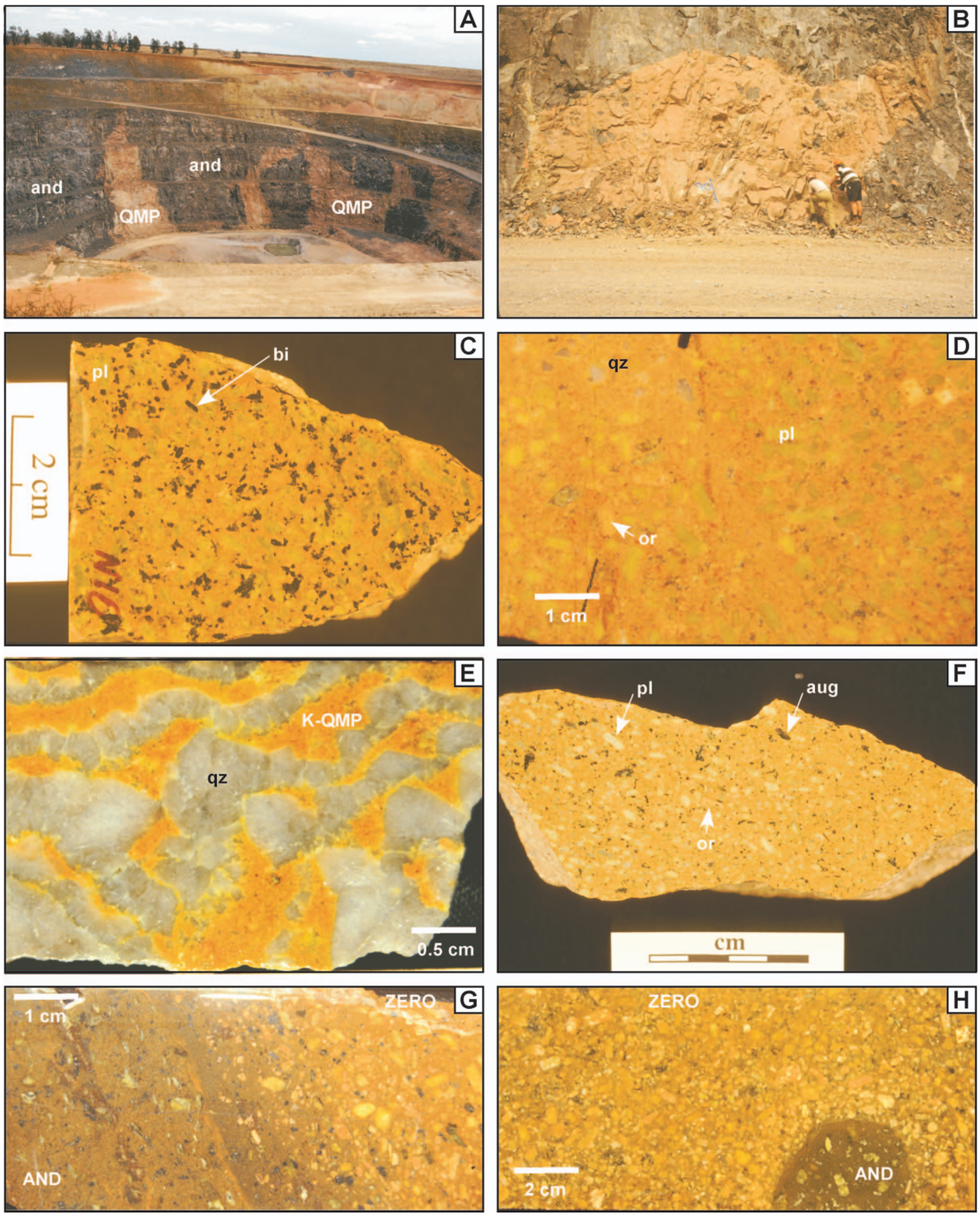

Downloaded by [Ondokuz Mayis Universitesine] at 17:04 13 November 2014

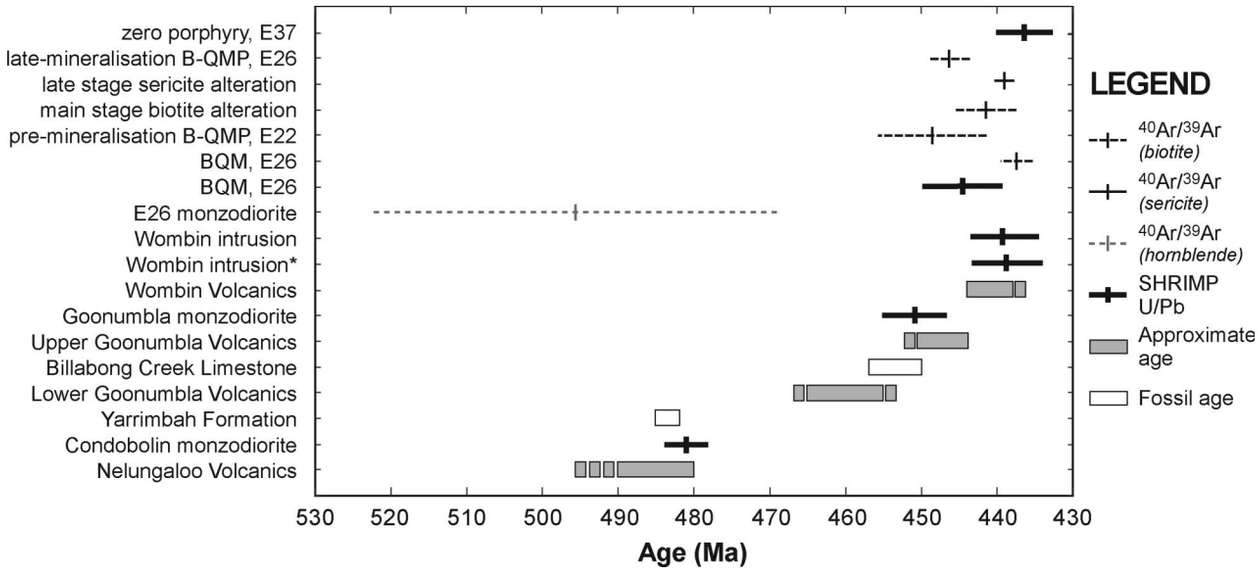

Figure 5 Geochronology of the Northparkes district, compiled from data and references in Table 1 as well as approximate volcanic rock and fossil ages from Duggan *et al.* (1999). Rock units are listed in terms of their relative ages from oldest to youngest; * is interpreted to be an intrusion into the Wombin Volcanics, not the Nelungaloo Volcanics as interpreted by Perkins *et al.* (1990); + approximate age is constrained by fossil and intrusive rock ages. Modified after Lickfold *et al.* (2003).

Goonumbla and Wombin volcanic rocks, and also for unmineralised intrusions emplaced within these units, these plots illustrate progressive enrichment in LILE (e.g. Ba and K) and depletion in Nb, Zr and Ti with time. However, the Lower Ordovician Nelungaloo Volcanics are notably enriched in La, Ce and P compared to the Goonumbla and Wombin Volcanics (Figure 8).

Mineralised intrusions

We describe the geochemistry of the mineralised intrusions at Northparkes in the same order as they are interpreted to have been emplaced (Lickfold *et al.* 2003), i.e. biotite–quartz monzonite (BQM) → early mineralisation biotite-phyric quartz monzonite porphyry (early-mineralisation B-QMP) → synmineralisation K-feldspar-phyric quartz monzonite porphyry (K-QMP) → augite + biotite + K-feldspar-phyric quartz monzonite porphyry (KA-QMP) → late-mineralisation biotite phyric quartz monzonite porphyry (late-mineralisation B-QMP). The geochemistry of the microgranite intrusions at E48, the monzodiorite intrusion at E26 and the basaltic trachyandesite and zero porphyry dykes at E26 are addressed separately.

BIOTITE–QUARTZ MONZONITE AND QUARTZ MONZONITE PORPHYRIES

The biotite–quartz monzonite and quartz monzonite porphyry intrusions have similar, though generally more felsic, compositions than their associated volcanic rocks. Despite selection of least-altered samples for chemical analyses, significant and unavoidable chemical modification has occurred during hydrothermal alteration. This is typically manifest as abundant, hematite-stained secondary K-feldspar in the quartz monzonite porphyry intrusions. Consequently, the mineralised intrusions plot at extreme K_2O contents on a K_2O *vs* SiO_2 classification diagram (Figure 7a). On the $Na_2O + K_2O$ *vs* SiO_2 diagram, the mineralised intrusions range from trachyte and trachydacite to rhyolite in composition (Figure 7b). Despite the effects of hydrothermal alteration, these plots show increasing

Figure 4 (a) E27 openpit northern wall showing the complex geometry of the pale-pink multiphase quartz monzonite porphyry (QMP) intrusions. The black trachyandesite host sequence has been pervasively biotite altered. (b) E27 openpit southwestern wall. Top of a low-angle quartz monzonite porphyry (KA-QMP) dyke that has intruded biotite-altered trachyandesite. Note the abundant mafic xenoliths close to the KA-QMP contact. (c) Underground sample of weakly porphyritic biotite quartz monzonite (BQM) intrusion from E26. Fine pink alkali feldspar has mantled coarser plagioclase (pl) phenocrysts. Biotite (bi) is the dominant mafic mineral. (d) Uncrowded (~35% phenocrysts) K-QMP intrusion from E27 (grab rock sample from one of the lower benches of the openpit). (e) E22 'brain rock' alternating bands of fine-grained K-feldspar-phyric quartz monzonite porphyry (K-QMP) that contains small (1–2 mm) phenocrysts of plagioclase and less commonly alkali feldspar and prismatic quartz crystals (E22/229 641.1 m). Some of the prismatic quartz bands are broken. (f) KA-QMP intrusion from E27, with conspicuous alkali feldspar and plagioclase phenocrysts, together with lesser augite (au), biotite and magnetite grains in a fine-grained K-feldspar–quartz–hematite-altered groundmass. (g) Gradational contact between basaltic trachyandesite and zero porphyry, E26 (E26/264 247.6 m). (h) Rounded clast of basaltic trachyandesite in a zero porphyry dyke (E26/264 263.0 m). Note the sparse plagioclase phenocrysts in the basaltic trachyandesite phase and the abundant plagioclase and alkali feldspar phenocrysts in the zero porphyry.

Downloaded by [Ondokuz Mayis Universitesine] at 17:04 13 November 2014

Downloaded by [Ondokuz Mayis Universitesine] at 17:04 13 November 2014

Table 2 Selected whole-rock major (XRF), trace (XRD) and rare-earth (solution ICP-MS) element analyses of unmineralised intrusions from the Northparkes district and intrusions related to the Northparkes porphyry Cu – Au deposits.

Rock type	E22 BQM	E22 B-QMP, early mineral	E22 K-QMP	E22 KA-QMP	E27 BQM	E27 B-QMP, early mineral	E27 K-QMP	E27 KA-QMP	E48 BQM	E48 Micro-granite	E48 K-QMP	E48 KA-QMP
Sample no	E22/229/728.6	E22/229/635.1	E22/205/400.9	E22/2/345.7	E27/28/709.0	E27/4/225.9	E27/11/73.6	E27/7/147.8	E48/13w2/970.7	E48/13W2/951.2	E48/15W1/651.3	E48/11/531.5
SiO_2	68.02	65.33	69.73	72.49	64.52	64.54	65.80	68.02	63.07	68.91	72.78	69.38
TiO_2	0.27	0.29	0.20	0.15	0.35	0.29	0.27	0.23	0.43	0.23	0.22	0.22
Al_2O_3	16.61	18.19	16.09	15.12	17.49	18.33	17.98	16.98	18.18	17.00	16.06	16.72
Fe_2O_3	2.18	1.90	0.85	1.19	3.48	2.87	1.72	2.56	5.06	0.34	0.91	0.54
MnO	0.07	0.04	0.04	0.03	0.07	0.03	0.03	0.04	0.05	0.01	0.01	0.01
MgO	0.68	0.91	0.63	0.36	1.24	1.00	0.90	0.77	1.88	0.39	0.93	0.52
CaO	1.83	2.75	1.80	1.15	2.16	2.29	1.69	1.66	1.73	0.54	1.23	0.55
Na_2O	3.86	4.61	2.97	3.72	4.95	5.83	4.88	4.53	5.01	3.02	1.90	2.38
K_2O	6.26	5.14	6.72	5.65	5.44	4.63	5.80	5.10	4.25	9.35	4.31	8.89
P_2O_5	0.11	0.15	0.06	0.04	0.20	0.10	0.10	0.08	0.27	0.07	0.04	0.07
Total %	99.60	99.49	99.65	99.59	99.48	99.63	99.70	99.63	99.63	99.97	100.00	99.72
LOI %	2.57	4.22	3.19	2.00	2.59	2.89	3.21	3.65	5.59	1.51	3.82	1.88
Ba	382	1102	961	598	655	1120	826	694	728	955	752	880
Rb	95	68	82	77.8	79	57	72	72	69.7	85.4	46.4	79.9
Sr	338	731	684	267	543	560	449	507	525	168	140	232
Pb	7	4	25	7	6	3	5	4	5	17	<1.5	7
Zr	195	73	86	91	147	77	77	77	126	82	67	76
Nb	10.5	3.8	4.8	4	7.7	4.0	3.5	3.7	8	3	3	3
Y	19	10	6	6	18	13	7	9	16	6	4	8
La	18	9	3	8	17	14	4	12	23	7	4	2
Ce	35	23	16	18	38	30	16	24	37	16	16	18
Nd	17	12	5	6	18	14	7	12	19	4	5	7
Sc	4	4	4	2	6	3	3	2	7	3	2	3
Cr	2	2	2	1	3	3	3	1	3	<1	1	1
Ni	1	1	1	<1	1	1	2	1	2	<1	2	1
Cu	744	5200	7000	795	778	590	6300	227	442	1050	12300	5500
Zn	36	40	103	39	50	20	24	31	60	22	1016	46
V	56	78	44	45	87	78	126	55	125	29	25	42
Sc	3.04	3.35	1.79	1.47	4.84	2.70	2.45	1.78	6.32	1.45	1.29	1.51
Rb	98.31	80.09	87.46	84.32	84.32	59.10	72.00	73.82	71.90	90.14	48.54	85.80
Sr	355.00	1478.00	736.00	287.00	566.00	516.00	416.00	496.00	496.00	183.00	161.00	261.00
Y	21.01	12.54	6.51	6.50	21.99	13.84	6.62	9.55	17.22	6.68	4.43	8.40
Zr	216.00	105.00	92.50	101.00	170.00	81.40	71.00	75.20	137.96	85.48	73.49	83.84
Nb	11.34	5.61	4.99	5.32	9.48	4.56	3.20	4.89	7.82	3.91	3.32	3.86
Mo	1.19	13.16	1.28	1.13	4.64	0.91	2.55	0.80	2.03	4.17	0.71	5.41
Sn	2.34	1.43	1.48	1.15	2.55	1.60	0.13	1.55	2.15	1.61	2.24	1.87

(*continued*)

Downloaded by [Ondokuz Mayis Universitesine] at 17:04 13 November 2014

Table 2 (*Continued*).

Rock type	E22 BQM	E22 B-QMP, early mineral	E22 K-QMP	E22 KA-QMP	E27 BQM	E27 B-QMP, early mineral	E27 K-QMP	E27 KA-QMP	E48 BQM	E48 Micro-granite	E48 K-QMP	E48 KA-QMP
Sample no	E22/229/728.6	E22/229/635.1	E22/205/400.9	E22/2/345.7	E27/28/709.0	E27/4/225.9	E27/11/73.6	E27/7/147.8	E48/13w2/970.7	E48/13W2/951.2	E48/15W1/651.3	E48/11/531.5
Sb	0.43	0.36	72.22	0.19	0.19	0.15	0.37	0.19	0.31	0.24	0.73	2.67
Cs	0.46	0.70	0.69	0.44	0.42	0.59	0.70	0.53	1.08	0.18	0.30	0.19
Ba	374.00	739.00	791.00	458.00	314.00	303.00	817.00	314.00	587.00	810.00	655.00	776.00
La	19.30	12.92	6.11	9.12	18.75	12.57	8.43	14.73	21.11	8.49	4.76	5.87
Ce	36.03	22.56	10.12	14.55	35.54	24.01	13.40	25.16	37.22	12.46	8.25	11.19
Pr	4.22	2.62	1.17	1.49	4.27	2.88	1.48	2.78	4.45	1.28	0.90	1.35
Nd	15.48	10.21	4.53	5.05	16.55	11.27	5.79	9.90	17.16	4.61	3.40	5.31
Sm	3.20	1.95	0.91	0.87	3.34	2.22	1.22	1.84	3.67	0.92	0.68	1.13
Eu	0.62	0.70	0.37	0.30	0.82	0.76	0.53	0.58	0.99	0.30	0.36	0.41
Gd	2.80	1.83	0.89	0.80	3.00	2.02	1.15	1.60	3.15	0.90	0.62	1.10
Tb	0.49	0.28	0.14	0.13	0.48	0.32	0.19	0.25	0.50	0.14	0.11	0.19
Dy	3.10	1.74	0.88	0.86	3.03	1.98	1.10	1.48	3.00	0.95	0.64	1.22
Ho	0.68	0.37	0.19	0.20	0.64	0.44	0.24	0.33	0.61	0.20	0.14	0.26
Er	2.14	1.18	0.61	0.65	2.09	1.34	0.74	1.01	1.91	0.65	0.50	0.85
Yb	2.58	1.30	0.75	0.92	2.29	1.46	0.88	1.26	2.06	0.76	0.59	1.00
Lu	0.42	0.21	0.15	0.17	0.36	0.24	0.15	0.21	0.33	0.13	0.11	0.17
Hf	5.35	2.55	2.49	2.89	3.90	1.90	2.09	2.24	3.49	2.17	1.90	2.03
Ta	1.14	0.68	0.70	0.91	0.88	0.51	0.48	0.57	0.77	0.76	0.59	0.75
Tl	0.30	0.22	0.31	0.18	0.16	0.16	0.22	0.22	0.18	0.20	0.14	0.31
Pb	8.01	15.51	26.87	7.64	5.10	4.05	4.74	3.77	5.11	19.10	3.17	8.46
Th	7.09	2.72	3.19	5.33	5.29	1.46	1.40	3.09	4.36	1.38	1.23	1.80
U	3.06	0.97	0.98	2.33	2.41	0.68	0.46	1.24	1.30	0.48	0.33	0.47
139 La_N	61.26	41.02	19.39	28.96	59.51	39.91	26.77	46.77	67.01	26.94	15.10	18.65
140 Ce_N	44.32	27.75	12.45	17.90	43.72	29.54	16.45	30.94	45.78	15.33	10.14	13.77
141 Pr_N	36.40	22.58	10.12	12.89	36.84	24.86	12.77	23.97	38.37	11.01	7.74	11.60
146 Nd_N	25.92	17.11	7.58	8.45	27.72	18.88	9.69	16.57	28.75	7.72	5.69	8.90
147 Sm_N	16.67	10.16	4.72	4.56	17.39	11.58	6.36	9.59	19.13	4.80	3.54	5.88
151 Eu_N	8.58	9.67	5.14	4.20	11.37	10.54	7.39	8.04	13.77	4.18	4.96	5.71
157 Gd_N	10.80	7.06	3.44	3.10	11.57	7.81	4.44	6.17	12.17	3.47	2.38	4.24
159 Tb_N	9.91	5.79	2.90	2.65	9.89	6.50	3.84	5.04	10.12	2.90	2.17	3.87
163 Dy_N	9.55	5.34	2.72	2.65	9.34	6.08	3.38	4.56	9.22	2.91	1.95	3.76
165 Ho_N	9.29	5.05	2.60	2.77	8.77	6.00	3.31	4.54	8.42	2.75	1.94	3.56
167 Er_N	10.06	5.55	2.85	3.07	9.81	6.30	3.48	4.76	8.98	3.07	2.36	4.00
172 Yb_N	12.40	6.24	3.60	4.43	10.99	7.01	4.23	6.07	9.91	3.63	2.82	4.82
175 Lu_N	12.87	6.61	4.53	5.22	11.14	7.32	4.65	6.62	10.09	4.17	3.47	5.21
Eu*	13.42	8.47	4.03	3.76	14.18	9.51	5.31	7.69	15.26	4.08	2.90	4.99
Eu/Eu*	0.64	1.14	1.28	1.12	0.80	1.11	1.39	1.05	0.90	1.02	1.71	1.14

(*continued*)

Downloaded by [Ondokuz Mayis Universitesine] at 17:04 13 November 2014

Table 2 (*Continued*).

Rock type	E26 Monzo-diorite	E26 BQM	E26 K-QMP	E26 KA-QMP	E26 B-QMP, late mineral	E26 Zero porphyry	E37 zero porphyry	Condobolin Rd monzodiorite CSG162[a]	Goonumbla Hill monzodiorite CGS11[a]	Goonumbla Siding monzodiorite CSG59B[a]	Cooks Myalls monzonite CSG189[a]	Gunningbland Forest monzonite VL 10–3[a]
Sample No	E26/46/1720.2	E26/287/220.3	E26/189/229.8	E26/286/184.0	E26/264/235.3	E26/264/263.0	E37/3/245.2[a]					
SiO_2	56.28	61.54	66.02	65.13	65.10	65.41	66.68	54.74	52.40	52.34	59.76	63.75
TiO_2	0.59	0.44	0.32	0.28	0.29	0.27	0.29	0.66	0.82	0.80	0.47	0.38
Al_2O_3	18.90	18.00	17.01	17.73	17.68	18.22	16.66	18.46	19.66	17.57	18.17	17.98
Fe_2O_3	6.47	2.94	0.79	1.50	1.87	2.77	2.92	9.07	8.13	9.29	5.51	4.03
MnO	0.11	0.02	0.01	0.03	0.04	0.08	0.05	0.18	0.21	0.19	0.17	0.23
MgO	2.69	1.88	0.64	0.94	0.92	1.26	1.60	3.11	3.36	4.32	2.05	1.18
CaO	6.40	4.39	1.34	3.34	2.71	2.03	1.96	8.03	7.27	7.60	4.77	2.88
Na_2O	4.76	5.21	2.86	5.10	5.48	4.49	4.15	3.31	4.26	3.33	4.68	5.31
K_2O	3.31	4.63	8.23	5.41	5.38	5.39	5.51	2.05	3.19	4.04	4.04	4.11
P_2O_5	0.44	0.27	0.09	0.11	0.09	0.08	0.10	0.37	0.57	0.42	0.29	0.15
Total %	99.97	99.14	101.06	99.98	99.56	99.91						99.60
LOI %	2.47	4.90	3.11	5.27	3.61	3.02	3.18	1.52	2.64	1.88	0.81	1.87
Ba	893	712	1064	1573	1113	1527	988	494	1124	949	842	852
Rb	54	70	82.1	55.3	48	83	83	23	53	54	58	80.1
Sr	1611	1211	811	1213	960	855	171	962	1731	1538	1016	1031
Pb	4	7	8	3	7	8	2	7	4	4	9	10
Zr	67	103	76	77	79	80	98	114	67	85	112	131
Nb	4.3	5.4	3	4	4.1	3.7	6.1	6.3	4.5	5.0	6.1	8
Y	17	15	4	10	12	12	12	20	20	20	18	18
La	15	11	5	9	11	13			0.0	0.0	0.0	14
Ce	32	33	13	26	26	30			0.0	0.0	0.0	32
Nd	17	15	8	11	12	15			0.0	0.0	0.0	13
Sc	12	9	5	4	4	2	4	21	14	20	10	5
Cr	4	5	2	6	2	2	5	10	6	21	9	3
Ni	3	4	2	1	1	1	2	8	5	13	6	2
Cu	329	5200	21 100	3300	3400	9	8	200	104	190	62	49
Zn	37	48	41	22	28	38	48	118	86	95	92	66
V	194	148	86	95	72	71	68	194	221	271	128	83
Sc	9.90	6.46	2.63	2.42	2.64	2.00	5.17	20.00	12.50	20.40	8.50	4.77
Rb	56.07	73.49	82.38	57.39	51.14	85.16	83.46	22.00	50.00	50.00	55.00	80.00
Sr	1671.00	1291.00	796.00	1209.00	991.00	856.00	151.27	908.00	1633.00	1437.00	972.00	940.00
Y	19.02	17.36	4.91	10.50	13.78	12.47	10.18	20.00	19.00	19.00	17.00	17.20
Zr	82.49	123.65	110.30	78.83	84.65	75.38	64.88	107.00	66.00	82.00	115.00	115.00
Nb	5.00	6.72	4.43	4.19	4.89	4.14	6.41	6.30	4.66	5.19	5.51	7.50
Mo	2.34	1.75	1.23	3.64	1.73	0.62	0.61	1.89	1.04	1.34	3.29	1.86
Sn	3.99	0.75	0.27	0.35	0.19	0.38	0.75	2.19	1.89	2.14	1.76	0.50
Sb	0.12	0.05	0.08	0.07	0.20	0.67	1.18	0.26	0.21	0.30	0.03	0.16
Cs	0.18	0.22	0.20	0.69	0.20	0.45	1.03	0.16	0.48	0.37	0.40	0.30

(*continued*)

Downloaded by [Ondokuz Mayis Universitesine] at 17:04 13 November 2014

Table 2 (*Continued*).

Rock type	E26 Monzo-diorite	E26 BQM	E26 K-QMP	E26 KA-QMP	E26 B-QMP, late mineral	E26 Zero porphyry	E37 zero porphyry	Condobolin Rd monzodiorite	Goonumbla Hill monzodiorite	Goonumbla Siding monzodiorite	Cooks Myalls monzonite	Gunningbland Forest monzonite
Sample No	E26/46/1720.2	E26/287/220.3	E26/189/229.8	E26/286/184.0	E26/264/235.3	E26/264/263.0	E37/3/245.2[a]	CSG162[a]	CGS11[a]	CSG59B[a]	CSG189[a]	VL 10–3[a]
Ba	867.00	742.00	851.00	1542.00	1204.00	1582.00	970.45	518.00	971.00	923.00	823.00	796.00
La	18.01	15.27	4.10	12.50	14.95	16.95	13.14	27.90	18.20	15.70	18.40	18.76
Ce	34.53	29.13	6.76	21.70	26.36	29.17	20.47	57.80	34.70	30.10	33.80	31.06
Pr	4.36	3.59	0.81	2.51	3.07	3.25	2.27	8.05	4.70	4.06	4.32	3.52
Nd	18.09	14.60	3.30	9.80	11.75	11.53	8.78	34.10	20.50	17.50	17.70	13.61
Sm	4.01	3.05	0.73	1.92	2.30	2.23	1.70	7.05	4.74	4.15	3.77	2.93
Eu	1.26	0.87	0.33	0.63	0.72	0.75	0.54	1.79	1.50	1.23	1.14	0.90
Gd	3.69	2.80	0.77	1.77	2.10	1.93	1.63	5.52	4.53	4.09	3.50	2.81
Tb	0.56	0.43	0.12	0.27	0.33	0.32	0.24	0.78	0.70	0.67	0.55	0.49
Dy	3.27	2.63	0.74	1.63	2.01	1.93	1.49	4.00	3.80	3.73	3.14	2.91
Ho	0.65	0.55	0.15	0.34	0.43	0.42	0.35	0.79	0.75	0.75	0.64	0.64
Er	1.91	1.65	0.52	1.05	1.30	1.30	1.11	2.26	2.21	2.27	2.04	1.99
Yb	1.79	1.68	0.63	1.08	1.41	1.48	1.29	2.13	1.97	2.13	2.08	2.29
Lu	0.27	0.26	0.12	0.17	0.23	0.23	0.22	0.34	0.31	0.34	0.34	0.37
Hf	2.09	3.14	2.78	2.00	2.05	2.01	2.00	3.09	2.01	2.45	3.24	3.36
Ta	0.52	0.62	0.92	0.58	0.57	0.45	0.45	0.48	0.39	0.44	0.53	0.63
Tl	0.18	0.19	0.33	0.17	0.12	0.30	0.02	0.05	0.10	0.15	0.11	0.20
Pb	5.71	8.02	9.39	5.68	7.71	9.61	3.36	8.05	6.30	7.01	9.83	12.20
Th	2.14	4.45	2.07	1.73	1.98	1.76	3.27	3.41	2.10	2.54	3.54	3.73
U	1.29	1.12	0.64	0.53	0.77	0.98	1.26	2.59	1.02	1.29	2.07	1.97
139 La_N	57.18	48.48	13.02	39.67	47.45	53.81	41.71	88.63	57.84	49.99	58.55	59.56
140 Ce_N	42.48	35.83	8.32	26.69	32.43	35.88	25.18	71.12	42.72	36.97	41.61	38.21
141 Pr_N	37.58	30.91	7.00	21.67	26.47	28.04	19.57	69.39	40.51	34.99	37.23	30.35
146 Nd_N	30.31	24.46	5.53	16.41	19.68	19.31	14.71	57.17	34.28	29.37	29.69	22.80
147 Sm_N	20.89	15.88	3.79	9.99	11.99	11.61	8.84	36.70	24.68	21.59	19.64	15.28
151 Eu_N	17.45	12.08	4.61	8.77	9.97	10.35	7.52	24.82	20.84	17.05	15.85	12.47
157 Gd_N	14.26	10.80	2.96	6.85	8.12	7.45	6.28	21.30	17.48	15.81	13.52	10.85
159 Tb_N	11.35	8.72	2.44	5.58	6.79	6.57	4.91	15.85	14.21	13.59	11.24	10.09
163 Dy_N	10.06	8.10	2.27	5.01	6.18	5.92	4.59	12.31	11.69	11.47	9.67	8.95
165 Ho_N	8.91	7.47	2.12	4.72	5.85	5.71	4.77	10.76	10.25	10.32	8.71	8.80
167 Er_N	8.98	7.74	2.42	4.95	6.10	6.11	5.19	10.60	10.39	10.67	9.57	9.33
172 Yb_N	8.62	8.08	3.04	5.21	6.78	7.10	6.20	10.22	9.48	10.23	10.02	11.02
175 Lu_N	8.33	7.97	3.80	5.19	7.27	7.26	6.66	10.47	9.58	10.59	10.43	11.37
Eu*	17.26	13.10	3.35	8.27	9.87	9.30	7.45	27.96	20.77	18.48	16.30	12.88
Eu/Eu*	1.01	0.92	1.38	1.06	1.01	1.11	1.01	0.89	1.00	0.92	0.97	0.97

SiO_2 to V are XRF analyses; Sc to Eu are ICP-MS analyses.
Eu*: Europium anomaly.
[a]Samples supplied by C. Simpson, North Ltd, 1999.

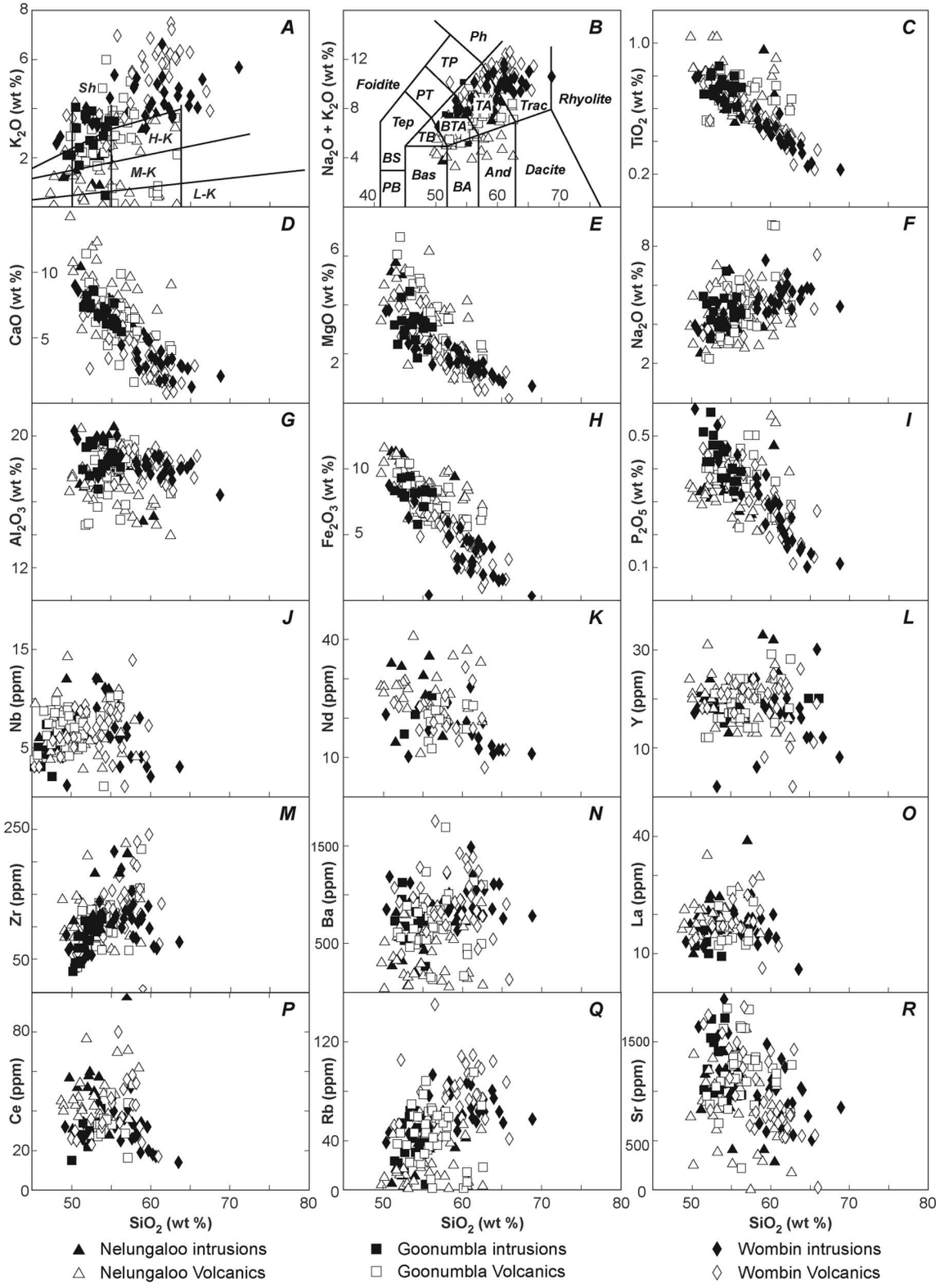

Figure 6 Harker diagrams for the volcanic and intrusive rocks of the Northparkes district. (a) K_2O *vs* SiO_2 (fields from Peccerillo & Taylor 1976); (b) $Na_2O + K_2O$ *vs* SiO_2 (fields from Le Bas *et al.* 1986); (c) TiO_2 *vs* SiO_2; (d) CaO *vs* SiO_2; (e) MgO *vs* SiO_2; (f) Na_2O *vs* SiO_2; (g) Al_2O_3 *vs* SiO_2; (h) Fe_2O_3 *vs* SiO_2; (i) P_2O_5 *vs* SiO_2; (j) Nb *vs* SiO_2; (k) Nd *vs* SiO_2; (l) Y *vs* SiO_2; (m) Zr *vs* SiO_2; (n) Ba *vs* SiO_2; (o) La *vs* SiO_2; (p) Ce *vs* SiO_2; (q) Rb *vs* SiO_2; (r) Sr *vs* SiO_2; And, andesite; BA, basaltic andesite; Bas, basalt; BS, basanite; BTA, basaltic trachyandesite; H-K, high-K; L-K, low-K; M-K, medium-K; PB, picrobasalt; Ph, phonolite; PT, phonotephrite; Sh, shoshonite; TA, trachyandesite; TB, trachybasalt; Tep, Tephrite; TP, tephriphonolite; Trac, trachyte.

Downloaded by [Ondokuz Mayis Universitesine] at 17:04 13 November 2014

Downloaded by [Ondokuz Mayis Universitesine] at 17:04 13 November 2014

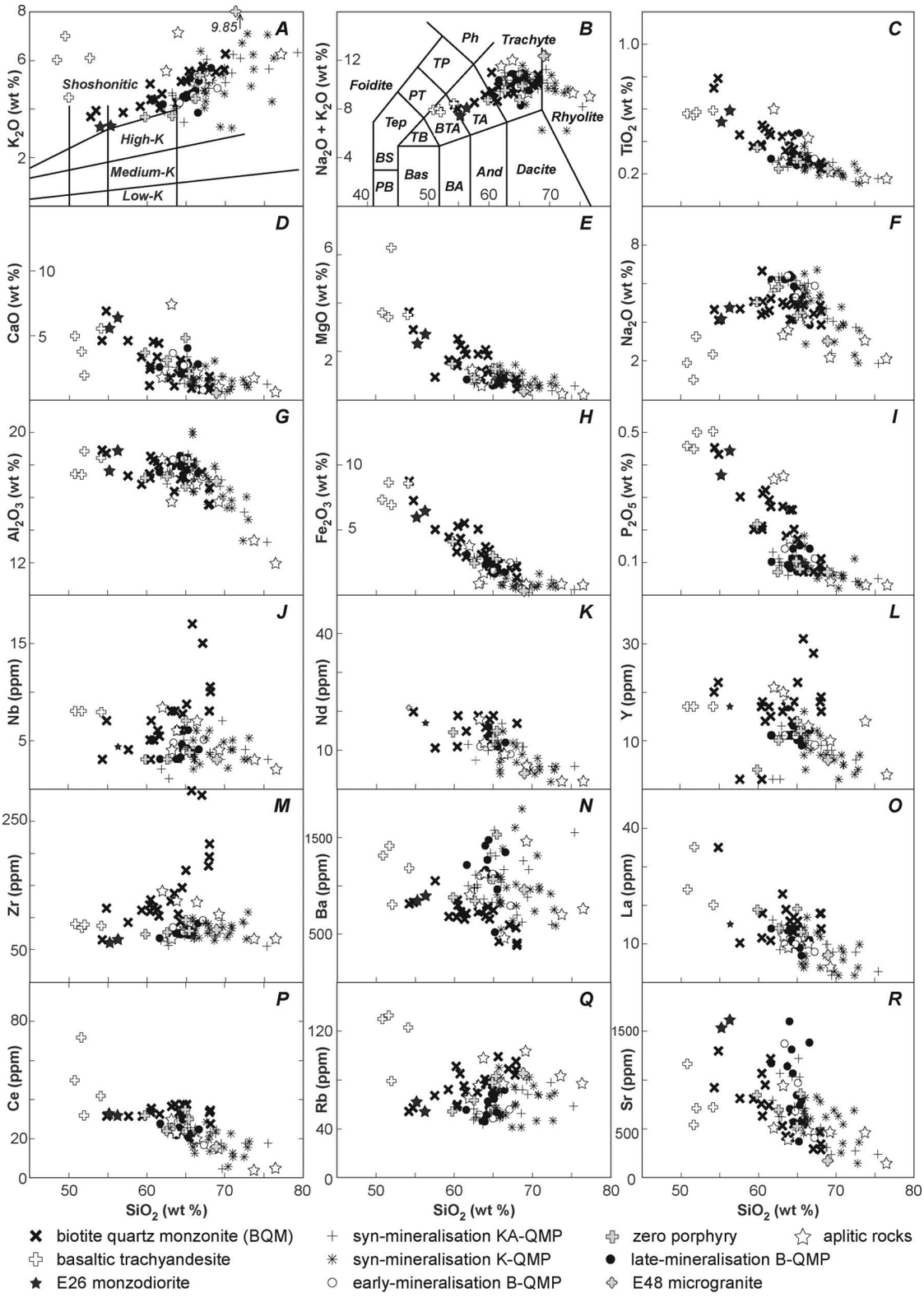

Figure 7 Harker diagrams for intrusive rocks associated with the Northparkes porphyry Cu–Au deposits; (a) K_2O *vs* SiO_2 (fields from Peccerillo & Taylor 1976); (b) $Na_2O + K_2O$ *vs* SiO_2 (fields from Le Bas *et al.* 1986); (c) TiO_2 *vs* SiO_2; (d) CaO *vs* SiO_2; (e) MgO *vs* SiO_2; (f) Na_2O *vs* SiO_2; (g) Al_2O_3 *vs* SiO_2; (h) Fe_2O_3 *vs* SiO_2; (i) P_2O_5 *vs* SiO_2; (j) Nb *vs* SiO_2; (k) Nd *vs* SiO_2; (l) Y *vs* SiO_2; (m) Zr *vs* SiO_2; (n) Ba *vs* SiO_2; (o) La *vs* SiO_2; (p) Ce *vs* SiO_2; (q) Rb *vs* SiO_2; (r) Sr *vs* SiO_2; And, andesite; BA, basaltic andesite; Bas, basalt; BS, basanite; BQM, biotite–quartz monzonite; B-QMP, biotite–quartz monzonite porphyry; BTA, basaltic trachyandesite; H-K, high-K; K-QMP, K-feldspar quartz monzonite porphyry; KA-QMP, K-feldspar–augite quartz monzonite porphyry; L-K, low-K; M-K, medium-K; PB, picrobasalt; Ph, phonolite; PT, phonotephrite; Sh, shoshonite; TA, trachyandesite; TB, trachybasalt; Tep, tephrite; TP, tephriphonolite.

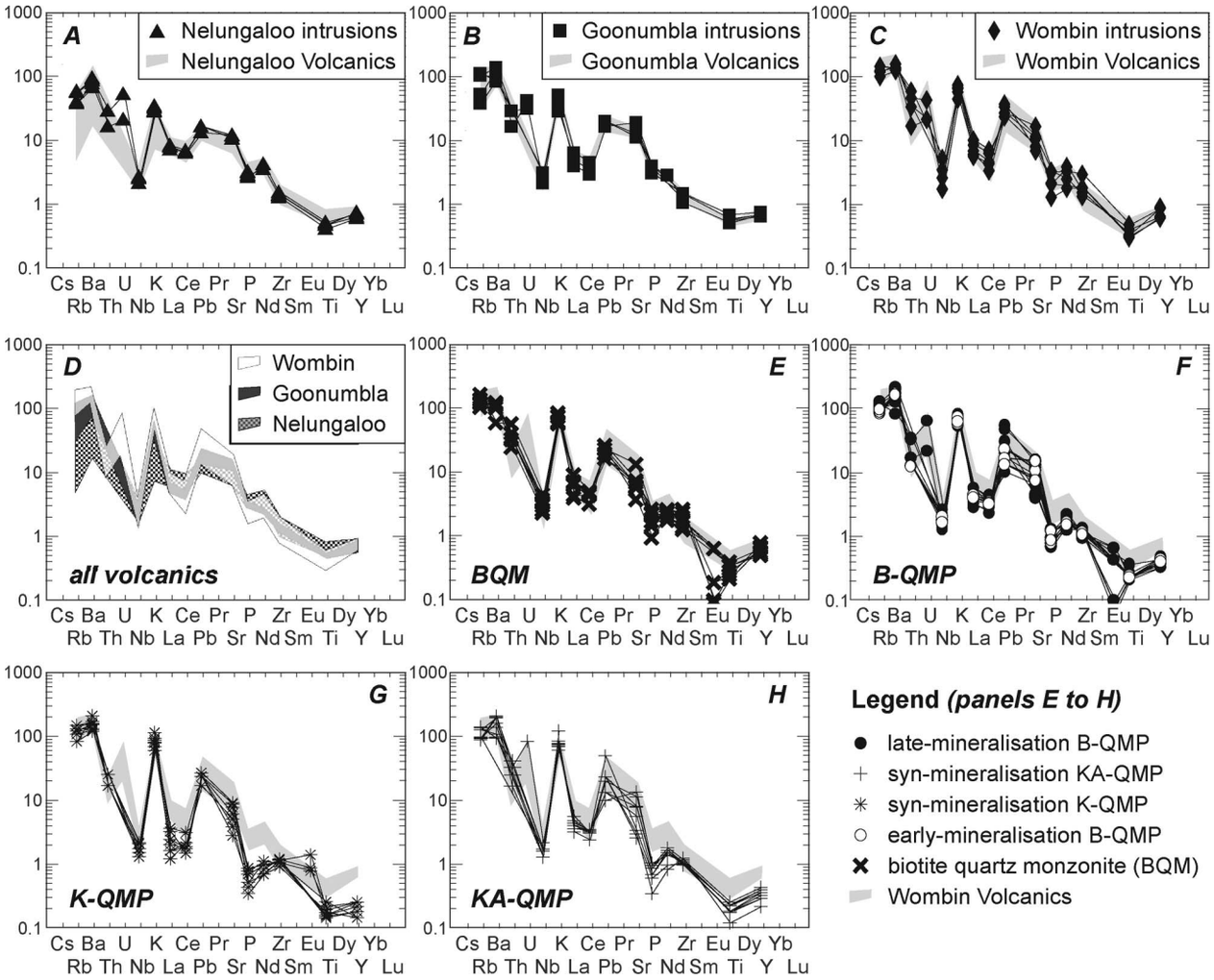

Figure 8 Multi-element plots for the volcanic and intrusive rocks of the Northparkes district normalised to N-MORB after Sun and McDonough (1989). (a) Nelungaloo; (b) Goonumbla; and (c) Wombin Volcanics (shaded fields) and related intrusions. (d) Comparative patterns for the three (early-, mid- and late-) Ordovician volcanic suites. (e) Biotite – quartz monzonite. (f) Early and late mineralisation biotite – quartz monzonite porphyry. (g) K-feldspar – quartz monzonite porphyry. (h) K-feldspar – augite – quartz monzonite porphyry. Data in (e – h) are plotted relative to the field defined by the Wombin Volcanics. BQM, biotite – quartz monzonite; B-QMP, biotite – quartz monzonite porphyry; K-QMP, K-feldspar – quartz monzonite porphyry; KA-QMP, K-feldspar – augite – quartz monzonite porphyry.

K_2O and $Na_2O + K_2O$ contents with increasing SiO_2 contents from early B-QMP to K-QMP intrusions. The KA-QMP have more variable SiO_2 contents, and include compositions more mafic than the K-QMP intrusions.

On SiO_2 *vs* TiO_2, Fe_2O_3, CaO and MgO plots (Figure 7), most of the BQM samples overlap the field defined by regional Wombin intrusions. In contrast, the quartz monzonite porphyry intrusions are notably more fractionated, extending the trends defined by the Goonumbla and Wombin Volcanics and their comagmatic intrusions to higher SiO_2 values. Note that although there is some scatter in the data, the later KA-QMP intrusions are generally not as fractionated, or as SiO_2-rich as the earlier formed K-QMP intrusions. Note also that the early and late mineralisation B-QMP intrusions cannot be distinguished on these plots. The B-QMP intrusions are the least evolved variety of quartz monzonite porphyry associated with the Northparkes deposits.

There are systematic decreases in P_2O_5 and Al_2O_3 with increasing SiO_2 contents (Figure 7). Al_2O_3 contents also decrease with decreasing MgO, although there is a notable change in slope at ~1% MgO, which is the upper limit of MgO content of the quartz monzonite porphyry intrusions (Lickfold 2002). Na_2O contents increase with fractionation until SiO_2 ~62%, after which there is a sharp decrease in Na_2O as SiO_2 increases (Figure 7f). When Na_2O is plotted against MgO, it initially increases as MgO decreases to ~1% and thereafter decreases with decreasing MgO contents (Lickfold 2002). The changes of slope in the Al_2O_3 and Na_2O trends at MgO ~1% may indicate K-feldspar replacement of albite in some quartz monzonite porphyry samples.

There is an overlap in trace-element compositions between the mineralised intrusions and some of the regional intrusive rocks in the Wombin Volcanics. For example, La, Ce and Nd abundances decrease with SiO_2

Downloaded by [Ondokuz Mayis Universitesine] at 17:04 13 November 2014

contents increasing beyond ~60%, especially in the early and late mineralisation B-QMP, K-QMP and KA-QMP intrusions (Figure 7). The relationship between SiO_2 and Ce is noteworthy. Ce abundances decrease slightly for the BQM intrusions, although they decrease markedly with increasing SiO_2 > ~60% for the quartz monzonite porphyries. Y abundances mimic Ce abundances with increasing SiO_2, although they are higher and more variable in the BQM intrusions than in the quartz monzonite porphyries (Figure 7). Ba and Sr in the BQM intrusions are typically lower, and Rb and Nb contents are higher than in the quartz monzonite porphyries for similar SiO_2 and TiO_2 contents (Figure 7).

Heithersay and Walshe's (1995) depleted Zr trend is most pronounced in the ore-related quartz monzonite porphyries and provides a distinct contrast with the BQM intrusions and the regional intrusive and volcanic rocks (Figures 6, 7). Zr abundances in the quartz monzonite porphyries decrease with decreasing MgO contents, whereas they increase with decreasing MgO contents in most of the BQM samples (Lickfold 2002). The latter pattern is similar to most of the Goonumbla and Wombin rocks.

Multi-element plots of intrusive compositions from the Northparkes porphyry deposits illustrate that with the exception of a negative Eu anomaly, the BQM intrusions are virtually identical to many of the intrusions associated with the Wombin Volcanics (Figures 8, 9). Progressive fractionation of incompatible and compatible elements from the Mid- to Late Ordovician Goonumbla and Wombin Volcanics and associated intrusions (including the BQM) appears to have become more pronounced with evolution of the quartz monzonite porphyry complex (Figures 8, 9).

Downloaded by [Ondokuz Mayis Universitesine] at 17:04 13 November 2014

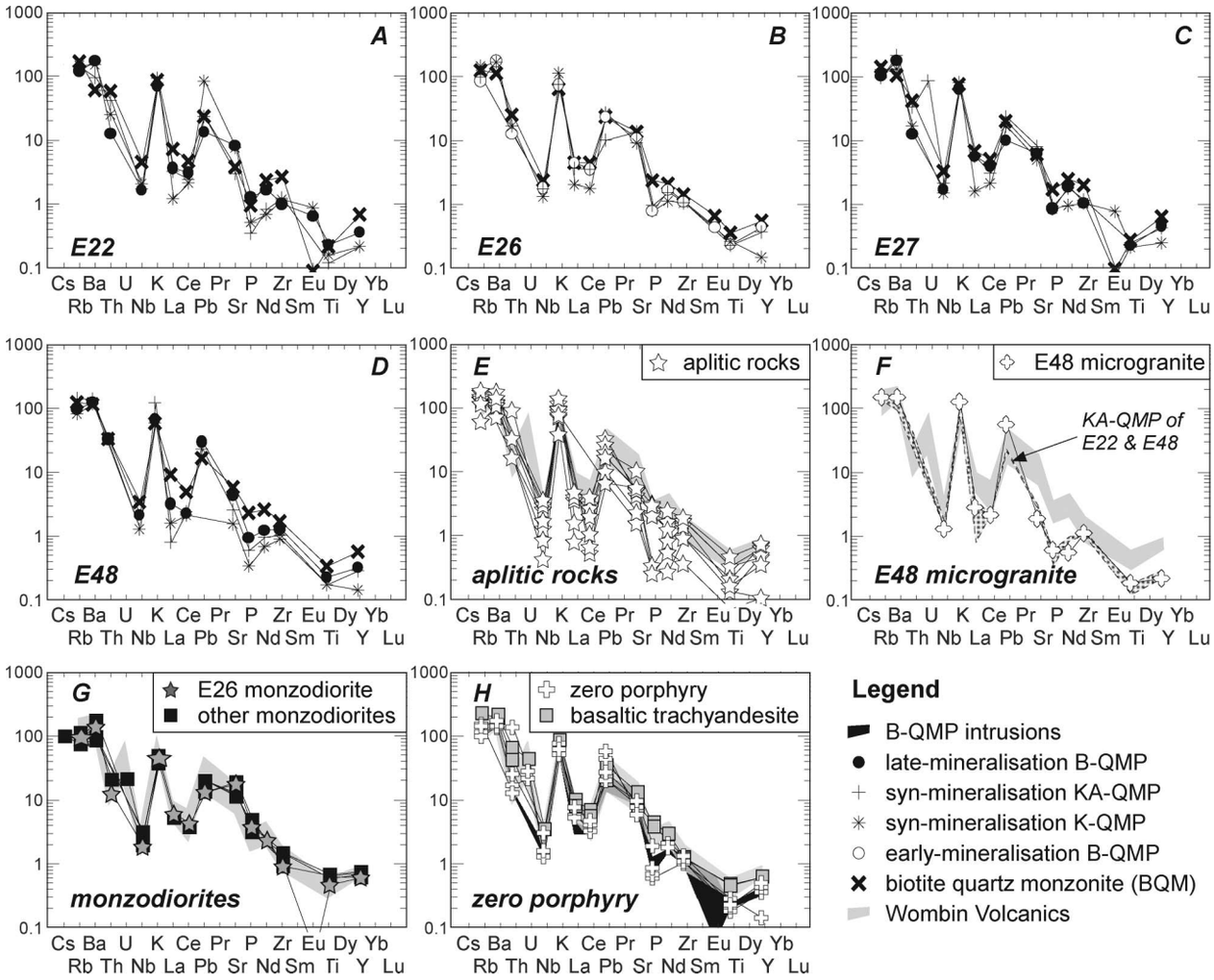

Figure 9 Multi-element plots for the intrusive rocks common to the Northparkes porphyry Cu – Au deposits studied: plotted per deposit for (a) E22; (b) E26; (c) E27; and (d) E48. Other intrusive rocks associated with the porphyry ore deposits are plotted relative to the field defined by the Wombin Volcanics: (e) aplite intrusions from all four deposits; (f) microgranite intrusion at E48 (the field defined by the KA-QMP intrusions at E22 and E48 is plotted for comparative purposes); (g) monzodiorite intrusion at E26 and from elsewhere within the Goonumbla Volcanics; and (h) basaltic trachyandesite and zero porphyry intrusions at E26 (the field defined by the B-QMP intrusions is plotted for comparative purposes). BQM, biotite – quartz monzonite; B-QMP, biotite – quartz monzonite porphyry; K-QMP, K-feldspar – quartz monzonite porphyry; KA-QMP, K-feldspar – augite – quartz monzonite porphyry.

Downloaded by [Ondokuz Mayis Universitesine] at 17:04 13 November 2014

MINOR INTRUSIONS

There are several texturally distinctive but volumetrically minor intrusions that have been identified at Northparkes. The monzodiorite intersected by deep drilling at E26 is the oldest known intrusion in the mine area. This rock cannot be discriminated geochemically from the Goonumbla volcanic and intrusive rocks (Figures 8, 9g), and it is interpreted here to be part of the Goonumbla Volcanics suite rather than the mineralised intrusive complex. In contrast, the microgranite intrusion at E48 most closely resembles the KA-QMP intrusions, particularly at E22 and E48 (Figures 7, 9f). The microgranite is therefore interpreted to be a derivative of a KA-QMP intrusion.

Two distinct groups of rocks constitute the volumetrically minor post-mineralisation zero porphyry dykes at E26: a marginal basaltic trachyandesite facies and a central K-feldspar-phyric mafic monzonite zero porphyry facies (Lickfold 2002; Lickfold *et al.* 2003) (Figure 4g, h). Whole-rock major- and trace-element plots show that the trachyandesites are compositionally distinct from the zero porphyries (Figures 7, 9h), even though the trachyandesites occur as a fine-grained, apparently 'chilled', margin to the central zero porphyry facies (Lickfold *et al.* 2003) (Figure 4g). The trachyandesites have shoshonitic compositions, and plot as basaltic trachyandesites in the area that Keith *et al.* (1998) defined as mafic alkaline rocks, i.e. more mafic than andesite and trachyandesite and more alkali-rich than basalt or picrobasalt. In contrast, the zero porphyries plot entirely within the compositional fields defined by the Northparkes quartz monzonite porphyries, and most closely resemble B-QMP intrusions compositionally (Figure 9h). In addition to the significant SiO_2 gap between these two rock types (Figure 7), Figure 9h shows that the basaltic trachyandesites are relatively more enriched in K, Ba, La, Ce and Sr and less depleted in Nb, Th, P and Ti than the zero porphyry dykes and the other ore-related intrusive rocks. The E26 zero porphyry dykes are similar geochemically, texturally and mineralogically to zero porphyry dykes at the nearby E37 prospect, and to monzonite porphyries at Gunningbland (Figure 2).

INTERPRETATION

The consistent overlap and similar character of geochemical trends for most major and trace elements are inferred to reflect the broadly comagmatic nature of the intrusive and volcanic rocks of the evolving Mid- to Late Ordovician high-K calc-alkaline to shoshonitic Northparkes Group. In terms of major elements, the Goonumbla and Wombin Volcanics, including the ore-related BQM intrusions, show a coherent trend from basaltic trachyandesite through trachyte (or their intrusive equivalents), with increasing SiO_2 and K_2O contents and decreasing TiO_2, Al_2O_3, Fe_2O_3, CaO and MgO contents. These trends continue from the volcanic rocks of the Northparkes Group and related intrusions through to the mineralised quartz monzonite porphyries, and are consistent with early, low-pressure fractionation of olivine and clinopyroxene, followed by later fractionation of plagioclase, Fe–Ti oxide and apatite (Gill 1981). There is a general increase in the extent of fractionation from the Middle Ordovician to the Late Ordovician–Early Silurian rocks, with the strongly mineralised K-QMP intrusions being the most evolved compositionally. The KA-QMP intrusions tend to contain slightly more variable SiO_2 contents and by the time of intrusion of the minor-volume late-mineralisation B-QMP dykes and later-still basaltic trachyandesite dykes and zero porphyries, mafic compositions become more evident.

Rare-earth element geochemistry

We have completed solution ICP-MS rare-earth element (REE) analyses at the University of Tasmania on 23 ore-related intrusive rocks and 22 intrusive and volcanic rocks from elsewhere in the district. A selection of these results is included in Table 2. All data are tabulated in Lickfold (2002).

NORTHPARKES GROUP AND RELATED INTRUSIONS

The Goonumbla Volcanics and comagmatic Goonumbla Hill and Goonumbla Siding monzodiorite intrusions have coherent LREE-enriched patterns with relatively flat HREE patterns (Figure 10). They show moderate LREE enrichment. The Goonumbla Volcanics and associated intrusions lack any significant Eu anomaly. Wombin Volcanics show REE patterns that are similar to those of the Goonumbla Volcanics (Figure 10). The most evolved Wombin Volcanics show a significant dip in MREE. The similar REE patterns of the Wombin intrusions and the Wombin Volcanics are consistent with a comagmatic origin.

MINERALISED INTRUSIONS

Chondrite-normalised (Sun & McDonough 1989) whole-rock REE patterns for most of the intrusive rocks associated with the Northparkes deposits are different from those of the intrusive rocks exposed elsewhere in the district (Figure 10). LREE enrichment becomes progressively more pronounced through the sequence of mineralised intrusions. This is reflected in the steepening LREE profiles in Figures 10 and 11. The BQM intrusions are virtually identical to the intrusions associated with the Wombin Volcanics, with the exception of having a slightly stronger negative Eu anomaly (Figure 10). In the younger intrusions, however, the Eu anomaly reverses and becomes progressively more positive from early mineralisation B-QMP to synmineralisation K-QMP. It then decreases again for the late mineralisation KA-QMP intrusions (Figure 10).

In addition to the Eu anomalies and steepening LREE slopes, the most obvious difference between the mineralised intrusions at Northparkes and the regional intrusive rocks is a progressive decrease in overall REE abundances through the sequence of increasing fractionation from BQM (which is similar to the Wombin Volcanics) through B-QMP to K-QMP. This trend is reversed by the KA-QMP, which typically has higher total REE abundances than the K-QMP

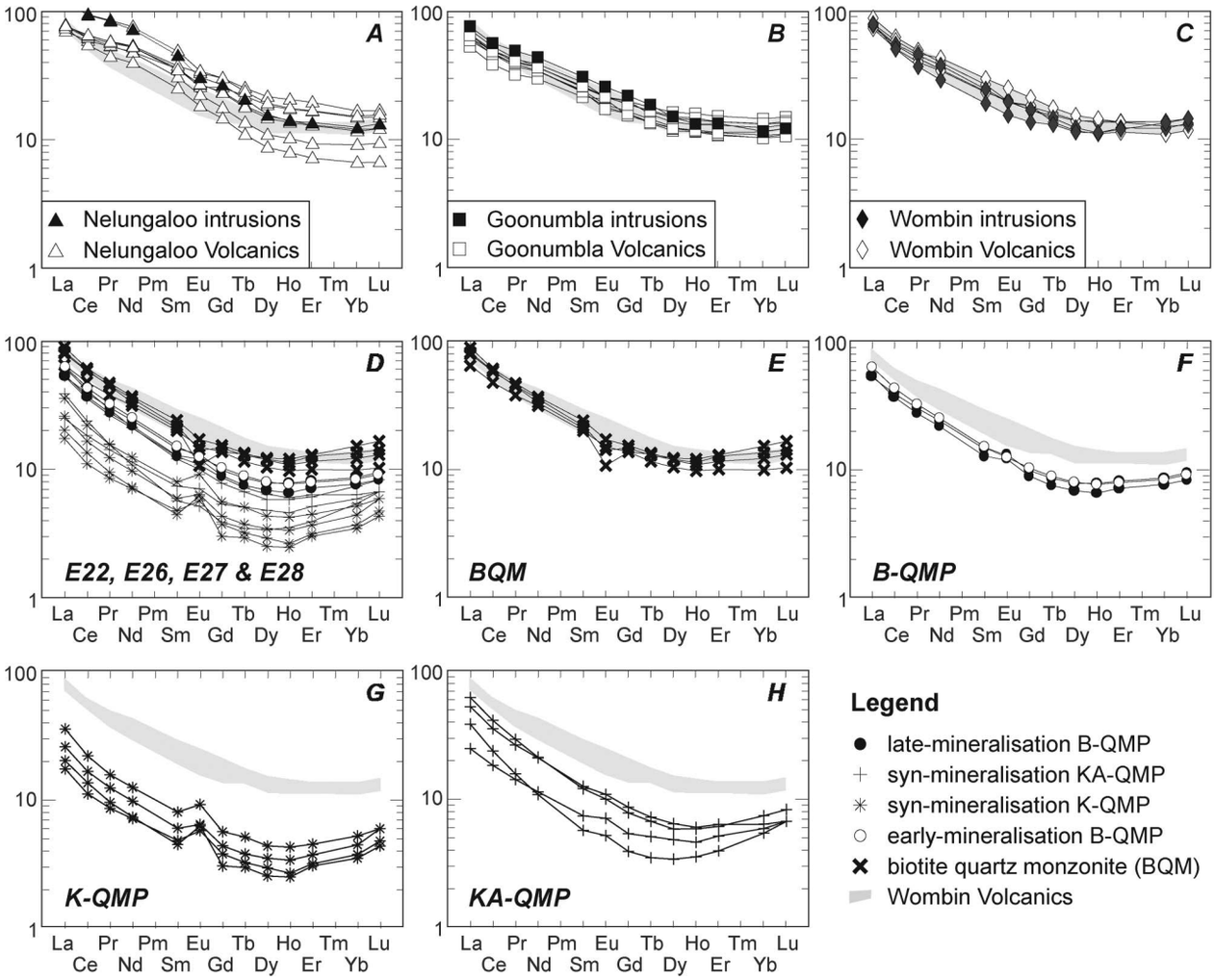

Figure 10 Chondrite-normalised (Sun & McDonough 1989) REE diagrams for the volcanic and intrusive rocks of (a) Nelungaloo; (b) Goonumbla; and (c) Wombin Volcanics. Also, the intrusive rocks associated with the Northparkes porphyry Cu – Au deposits (d) collectively; and separately (e) E22; (f) E26; (g) E27; and (h) E48. BQM, biotite – quartz monzonite; B-QMP, biotite – quartz monzonite porphyry; K-QMP, K-feldspar – quartz monzonite porphyry; KA-QMP, K-feldspar – augite – quartz monzonite porphyry.

Downloaded by [Ondokuz Mayis Universitesine] at 17:04 13 November 2014

intrusions (Figure 11). HREE depletion was more pronounced than LREE depletion, meaning that REE patterns become more U-shaped with fractionation, so that a trough is apparent between Eu and Ho, particularly for the strongly mineralised K-QMP intrusions. This relationship has been detected at all four Northparkes porphyry deposits (Figure 11). It discriminates them from geochemically similar Wombin intrusions such as the Gunningbland monzonite porphyry, which do not show the REE depletion characteristic of the ore-related intrusions (Figure 11e).

The REE patterns of the mineralised porphyries at Northparkes reflect progressive depletion in total REE abundances with increasing magmatic fractionation. All of the intrusions are LREE-enriched, but the relative LREE enrichment becomes more pronounced through the mineralised intrusive sequence. From the BQM intrusions, which have virtually identical REE patterns (with the exception of slightly stronger negative Eu anomalies) to the Wombin monzonites, the quartz monzonite porphyry intrusions are progressively depleted in MREE and HREE with increasing fractionation. However, HREE depletion was less pronounced than MREE depletion, giving rise to the distinctive U-shaped patterns in the most fractionated rocks, the synmineralisation K-QMP intrusions, which are also most intimately associated with high-grade ore formation. The late mineralisation KA-QMP and zero porphyry intrusions have less evolved compositions than the K-QMP intrusions and have less depleted REE compositions (Figure 11). This reversal with time towards less fractionated intrusive compositions cannot be explained by simple models of progressive fractionation, as has been advocated for the evolution of intrusive complexes in other porphyry mineral districts (Lang & Titley 1998).

INTERPRETATION

There are significant differences in trace-element abundances between the BQM and the mineralised quartz

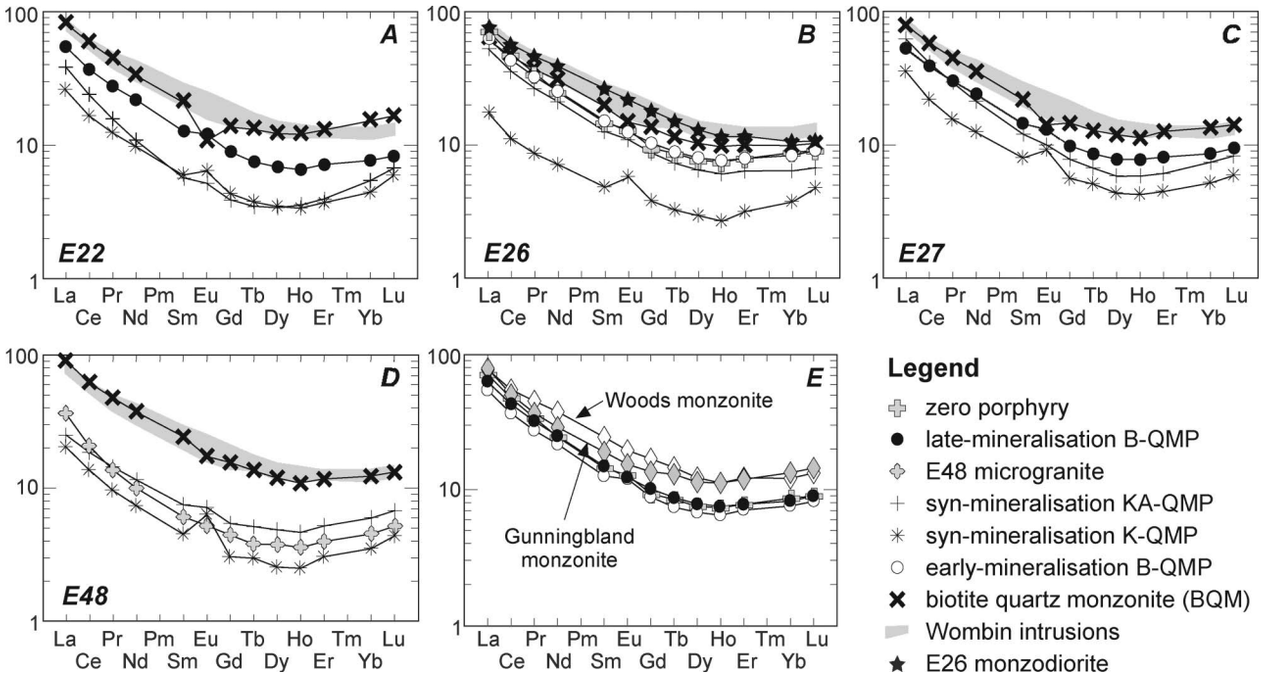

Figure 11 Comparative chondrite-normalised (Sun & McDonough 1989) REE diagrams for intrusions from (a) E22; (b) E26; (c) E27; and (d) E48. (e) Comparison of early and late mineralisation biotite – quartz monzonite porphyry intrusions from E22 and E26 with the E26 zero porphyry and unmineralised Gunningbland and Woods porphyry intrusions. BQM, biotite – quartz monzonite; B-QMP, biotite – quartz monzonite porphyry; K-QMP, K-feldspar – quartz monzonite porphyry; KA-QMP, K-feldspar – augite – quartz monzonite porphyry.

monzonite porphyries (e.g. higher Y, Nb and Zr and lower Ba in the BQM). These, combined with the fact that the KA-QMP and late mineralisation B-QMP intrusions are both younger and less evolved compositionally than the K-QMP intrusions, indicate that fractional crystallisation from a BQM-type magma could not have produced the observed sequence of mineralised intrusions. This contrasts with the model of Lang and Titley (1998) and contradicts the genetic model of Heithersay and Walshe (1995) for the E26 deposit, where the K-QMP intrusion was inferred to be a more fractionated apophysis derived from the shoulder of the BQM intrusion.

Eu anomalies in the volcanic and related intrusive rocks of the Northparkes Group are negligible (Figure 10). However, all intrusive rocks associated with the Northparkes deposits have positive or negative Eu anomalies (Figures 9, 10). Initially, a variably negative Eu anomaly characterises the BQM intrusions. Since the removal of feldspar from a felsic melt can result in the formation of a negative Eu anomaly (Green 1980), feldspar removal from the parental magma during fractional crystallisation may have been important for this anomaly in the BQM. However, the Eu anomaly in the more evolved quartz monzonite porphyries becomes progressively more positive with fractionation. Because feldspars are abundant in all volcanic and intrusive rocks of the Northparkes district, including the mineralising intrusions, it is thought unlikely that feldspar fractionation (or accumulation) alone could account for the variable nature of the Eu anomaly in the latter rocks, especially the less positive anomaly characteristic of the post K-QMP intrusions. It is possible that the Eu anomaly in the ore-related intrusions may have been influenced by an increase in oxygen fugacity during fractional crystallisation (McKay 1989). However, the lack of a Eu anomaly in the post-mineralisation zero porphyry, which contains anhydrite phenocrysts (evidence of oxidising conditions), suggests instead that changes in the source(s) of the melts and/or processes in the source regime may have been responsible for Eu variations in the mineralised intrusive complexes at Northparkes.

Trends of increasing K_2O and decreasing TiO_2, MgO, etc., with increasing SiO_2 from the BQM to the quartz monzonite porphyry intrusions, indicate some role for crystal fractionation from a BQM-type magma in the formation of the ore-related quartz monzonite porphyry intrusions at Northparkes. But the decrease in total REE abundances with increasing fractionation in the mineralised quartz monzonite porphyry complexes cannot be accounted for by simple plagioclase – K-feldspar – quartz ± augite ± biotite ± Fe – Ti-oxide fractionation, since removal of these very REE-poor phases would strongly enrich REE in residual liquids. Accessory phases such as apatite, sphene and zircon can strongly fractionate REE in magmatic systems. LREE and MREE are important components of apatite and sphene, and HREE are significant in zircon and less so in apatite (Bea 1996). Thus, removal of these minerals may have resulted in variable and significant REE depletion in the residual melt. Because most of the barren and mineralised intrusive rocks in the Northparkes district contain REE-rich accessory phases, it is

Downloaded by [Ondokuz Mayis Universitesine] at 17:04 13 November 2014

Downloaded by [Ondokuz Mayis Universitesine] at 17:04 13 November 2014

possible that their fractionation may have affected overall REE abundances.

Lickfold (2002) modelled the possible effects of fractionation of REE-rich and other phases in an attempt to explain the distinct decrease in REE abundances from the hornblende-bearing BQM to the mineralised quartz monzonite porphyries at Northparkes. She found that it was not possible to reproduce the REE compositions of the quartz monzonite porphyries by fractional crystallisation of the BQM magma to 10%, 30% or 50% by weight. Hornblende fractionation was also found to have virtually no effect on the bulk magmatic composition, with the exception of the development of a weak positive Eu anomaly, implying that hornblende crystallisation was unimportant for REE fractionation from the BQM to the K-QMP melts. Fractionation models involving potential REE-enriched phases (e.g. apatite, zircon, sphene, allanite) produced patterns that were too enriched in LREE for fractionation alone to account for the overall depletion in LREE abundances in the more evolved K-QMP rocks. The shortfall in the LREE therefore requires an alternative explanation.

Aqueous phase separation from a crystallising subvolcanic intrusion occurred during Cu–Au ore formation at Northparkes (Heithersay & Walshe 1995; Lickfold *et al.* 2003) and could help to explain the REE characteristics of the mineralising intrusions. Aqueous fluids containing $Cl \pm F$ can play a significant role in the fractionation of REE in halogen-enriched, water-saturated magmas (Baldwin & Pearce 1982; Candela 1984, 1990; Webster *et al.* 1989; Smith *et al.* 1999). Candela (1984) proposed that in the presence of a volatile-rich phase, LREE and, to a lesser extent, MREE partition preferentially into the volatile-rich phase, leaving the residual melt relatively depleted in LREE and, to a lesser extent, MREE and HREE. Field examples that demonstrate the role of volatile-induced REE mobilisation in magmatic–hydrothermal environments include Carten *et al.* (1988), Hassanen (1997) and de Hoog and van Bergen (2000).

Primary accessory F-rich phlogopite and fluorapatite phenocrysts occur in the quartz monzonite porphyry intrusions at Northparkes (Müller *et al.* 1994; Heithersay & Walshe 1995; Lickfold 2002), and fluorite occurs in the main (minor) and late-stage alteration assemblages (Lickfold *et al.* 2003). These features indicate that fluorine was an important component of the magmas and hydrothermal fluids at Northparkes. Also, the presence of hypersaline fluid inclusions (Heithersay & Walshe 1995; Lickfold *et al.* 2003) provides evidence for the involvement of Cl-rich brines in the mineralising process (Lickfold *et al.* 2003). F and Cl therefore could have played a role in REE mobility in the Northparkes intrusions, although we are not able to quantify their effects on the compositional evolution of the monzonites.

DISCUSSION

Mafic alkaline magmas and porphyry ore formation

The coexistence of zero porphyry monzonite and trachyandesite in the same dykes (Figure 4g) provides physical evidence of coexistence of mafic and silicic alkaline magmas during the final stages of magmatism at Northparkes. The abundance of mafic xenoliths and less evolved chemical compositions in the KA-QMP intrusions provide evidence for mafic magma involvement during mineralisation.

Mantle-derived mafic alkaline magmas and shoshonites have been proposed to contribute metals (especially Au) and volatiles to a spectrum of magmatic–hydrothermal ore deposits (Richards 1997; Sillitoe 1997; Jensen & Barton 2000), including several porphyry deposits (Keith *et al.* 1993, 1997, 1998; Rowland & Wilkinson 1999; Hattori & Keith 2001; Maughan *et al.* 2002; Pollard & Taylor 2002; Halter *et al.* 2005). Keith *et al.* (1998) proposed that underplating or injection of wet oxidised mafic alkaline magma into a felsic magma chamber could have several possible consequences. The mafic alkaline magma may provide heat, which would promote convection and the subsequent turnover of magma to deliver undissolved volatiles from the felsic magma to the top of the magma chamber. Quenching of the mafic alkaline magma on contact with the cooler felsic magma could initiate the formation of a buoyant stream of volatile-rich magma and bubbles, thereby augmenting the supply of volatiles (and metals) to the top of the magma chamber. Note that in these models, ore-forming components are inferred to have been derived from both magmas (Keith *et al.* 1998; Hattori & Keith 2001; Maughan *et al.* 2002).

Recent volcanic eruptions highlight the probable operation of convective volatile-transfer mechanisms between basaltic magmas and overlying silicic magmas (Pallister *et al.* 1996; Kress 1997; Keith *et al.* 1998; Coombs *et al.* 2000; Cole *et al.* 2001). Anders *et al.* (1991) demonstrated that in the recent eruptions of two Chilean volcanoes, 50–100 times more S was emitted than could be accounted for by the volume of silicic magma erupted. Other recent volcanic eruptions emitting excess S (at least 20 times greater than melt solubility) include Ruiz (Fournelle 1990) and Pinatubo, where, in the latter case, excess S was present as SO_2 vapour and anhydrite crystals (Pasteris 1996). Kazahaya *et al.* (1994) documented excess SO_2 and H_2O emissions in recent eruptions of the Izu-Oshima volcano in Japan and suggested that since the Izu-Oshima magma was water-undersaturated and relatively reduced (containing no anhydrite), degassing of excess SO_2 and H_2O may have relied on magma convection driven by the increase in density of the magma after degassing (cf. Shinohara *et al.* 1995).

GENETIC MODEL FOR THE NORTHPARKES PORPHYRY DEPOSITS

A change from trachyandesitic (Goonumbla Volcanics) to trachytic shoshonitic magmatism (Wombin Volcanics) was the magmatic precursor to mineralisation at Northparkes. Critical ingredients that led to ore formation include: (i) a deep crustal structure that tapped shoshonitic melts from the mantle; (ii) a fractionating BQM-like magma chamber interacting with a mafic alkaline magma; and

(iii) cross-cutting northwest- and northeast-trending shallow crustal fault sets that localised the mineralised monzonite pipes. Based on these speculations, we propose the following model for the formation of the porphyry Cu–Au mineralised intrusions at Northparkes.

Prior to main stage mineralisation, emplacement of Late Ordovician to Early Silurian shoshonitic BQM-style melt into the shallow crust was most likely facilitated by deep-seated fault systems (Figure 12a). The BQM and equivalent regional intrusions may be smaller apophyses from a large, shallow-crustal magma

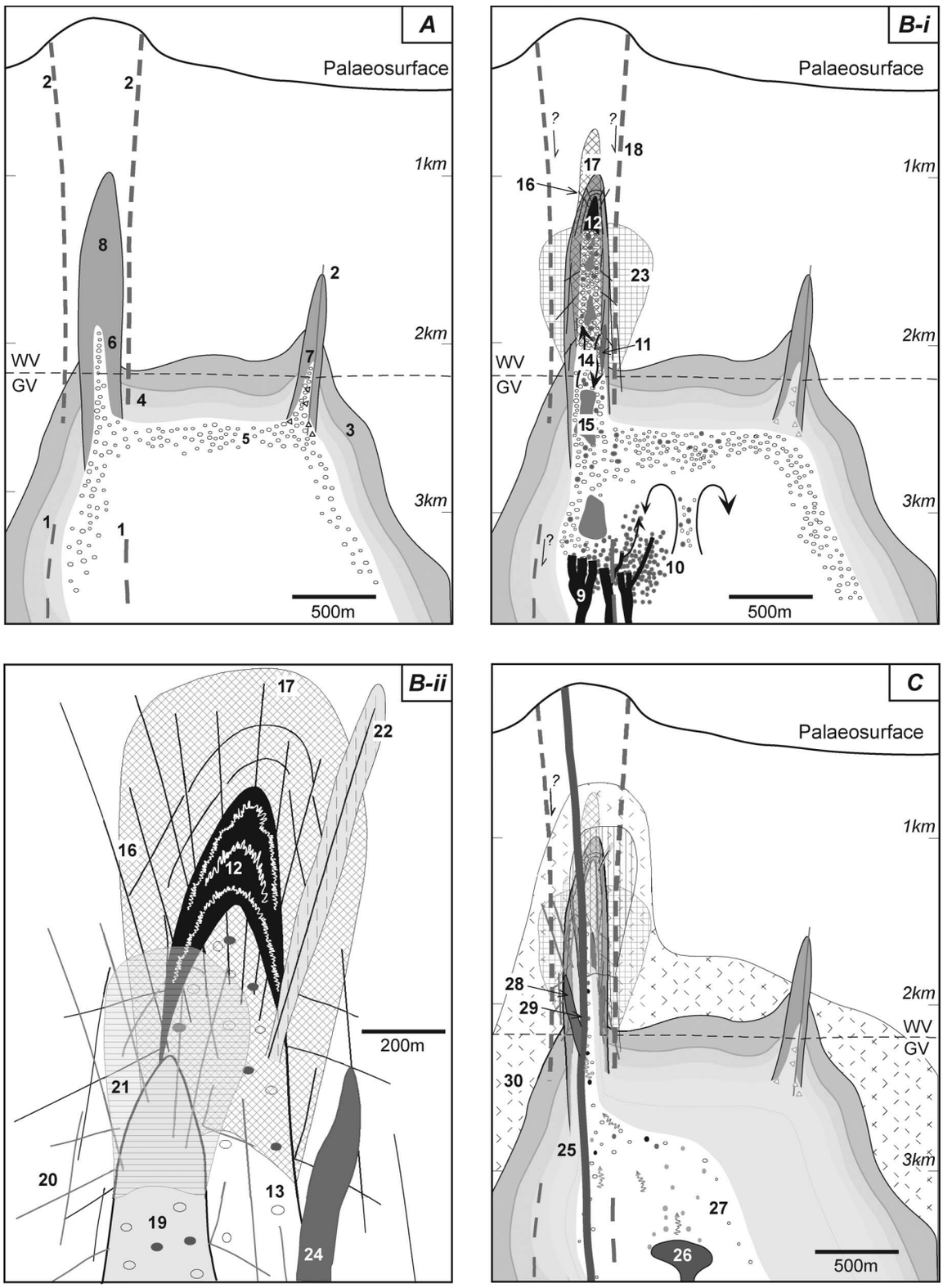

Downloaded by [Ondokuz Mayis Universitesine] at 17:04 13 November 2014

Downloaded by [Ondokuz Mayis Universitesine] at 17:04 13 November 2014

chamber. Fractional crystallisation may have caused some volatile exsolution during BQM emplacement, resulting in biotite–magnetite–K-feldspar alteration and associated sub-ore grade Cu–Au and Zn mineralisation of the volcanic wall-rocks that surround some BQM intrusions (e.g. the E31 prospect: Arundell 1998) (Figure 2).

The three early to syn-mineralisation phases comprising the pipe-like quartz monzonite porphyry complexes central to each of the Northparkes porphyry deposits (early mineralisation B-QMP → K-QMP → KA-QMP) were emplaced after the BQM intrusions (Figure 12b). Exsolution of a magmatic aqueous phase from the K-QMP and KA-QMP intrusions is inferred to have caused excessive LREE depletion and the distinctive U-shaped REE patterns (Figure 11). We speculate that the formation of the K-QMP and related intrusions was triggered by delivery of mafic alkaline melt to the base of the BQM magma chamber (Figure 12b). This would have allowed fertilisation of the magma chamber through the addition of excess volatiles and metals to the BQM melt, as outlined above. Seismic ruptures on shallow crustal fault systems above the magma chamber, such as the northwest- and northeast-trending fractures, are thought to have facilitated magma-chamber decompression, resulting in the simultaneous egress of an aqueous fluid and melt into dilatant zones. This resulted in the formation of the K-QMP and KA-QMP pipes that contain unidirectional solidification textures and miarolitic cavities, and also the Cu–Au mineralised stockwork and sheeted veins, and related K-silicate alteration assemblages.

Continued release of batches of quartz monzonite, combined with delivery of additional volumes of mafic alkaline melt to the base of the shallow crustal magma chamber, is believed to have eventually resulted in the reversal of fractionation trends from the K-QMP through KA-QMP to the late mineralisation B-QMP and post-mineralisation zero porphyry (Figures 11, 12b, c). The post-mineralisation zero porphyry dykes at E26 are interpreted to be near-mine examples of the final stage of widespread alkaline magmatism in the Late Ordovician–Early Silurian (Figure 12c). This is supported by the occurrence of similar post-mineralisation monzonite intrusions at E37 and by similar dykes at Gunningbland (Figure 2). The sharp intrusive contacts between the basaltic trachyandesite dykes and the surrounding BQM at E26 (Figure 4g) indicate that the BQM magma was crystalline at the time of basaltic trachyandesite intrusion. However, gradational contacts between the basaltic trachyandesite and monzonitic zero porphyry dykes, and the presence of rounded to angular clasts of basaltic trachyandesite in the younger zero porphyry intrusions (Figure 4h) indicate that the zero porphyry melt intruded the cores of the basaltic trachyandesite dykes before they were completely crystalline. These latter contact relationships are indicative of magma commingling (Keith *et al.* 1998). The basaltic trachyandesite and monzonitic melts are inferred to be different magmas derived from a broadly similar parental shoshonitic (basaltic) magma by different extents of fractionation (although with variable K_2O). In this scenario, episodic movement on deep-seated crustal faults may have triggered the roughly simultaneous intrusion of basaltic trachyandesitic and

Figure 12 Three-stage model for the formation of the Northparkes porphyry Cu–Au deposits. (a) Stage 1: Late Ordovician–Early Silurian magmatism and formation of a biotite–quartz monzonite (BQM) magma chamber and subeconomic Cu–Au mineralisation and related hydrothermal alteration. Seismic ruptures on deep-seated faults (1) and shallow-crustal NW- and NE-trending fracture systems (2) facilitated the intrusion of a subvolcanic monzonitic magma chamber at its neutral buoyancy level (~4 km?). Early albite–sericite alteration (3) formed around the magma chamber at this time. Crystallisation led to the formation of a zoned magma chamber (4) and volatile build up due to second boiling (5). When hydrostatic pressure exceeded lithostatic load and the tensile strength of the surrounding rocks, fracturing occurred, allowing intrusion of more fractionated BQM stocks (6 and 7) and formation of early biotite–K-feldspar alteration and related subeconomic Cu–Au mineralisation (8). (b–i and ii) Stage 2: Quartz monzonite porphyry formation and Cu–Au porphyry mineralisation. Seismic ruptures on deep-seated faults triggered the emplacement of mafic alkaline magmas (9) into the base of the BQM magma chamber. The mafic magma was quenched upon contact with the cooler BQM melt, initiating the formation of a buoyant stream of volatile-rich magma and bubbles of volatiles (10). This triggered intrusion of early mineralisation B-QMP dykes (11). As volatile production increased, the main episode of K-QMP melt formation occurred, with K-QMP melts intruding into dilatant sites in the shallow crust simultaneous with the ingress of abundant magmatic aqueous fluid, resulting in the formation of USTs and miarolitic cavities throughout the K-QMP intrusions (12 and 13). Localised fracturing and continued exsolution of magmatic aqueous fluid, possibly facilitated by the density contrast between buoyant, ascending, volatile-rich magma (14) and descending, relatively dense degassed magma (15; Shinohara *et al.* 1995) led to the formation of the thin K-QMP pipes and associated Cu–Au-bearing quartz vein array (16) and intense K-silicate alteration (17). Repeated fault movements (18) allowed for additional batches of mafic alkaline magma to be delivered to the base of the hybrid magma chamber, resulting in the formation of the KA-QMP intrusions (19) and their related quartz–sulfide stockwork vein arrays (20) and K-silicate alteration assemblages (21). Proximal phyllic (22) and distal propylitic alteration assemblages and carbonate–base-metal sulfide veins (23) formed after the KA-QMP intrusions and prior to the emplacement of the late stage B-QMP intrusions (24). (c) Stage 3: Intrusion of commingled basaltic trachyandesite and mafic monzonite porphyry dykes. During the waning stages of latest Ordovician–Early Silurian magmatism, near simultaneous intrusion of basaltic trachyandesite (25) and trachytic melts (26) occurred. This could have triggered first boiling and migration of aqueous fluid by advection through spanning clusters, because of the high viscosity of the near-fully crystallised magma chamber (27), leading to the intrusion of zero porphyry mafic monzonite dykes (28) and trachyandesite (29). Contact relationships imply that the two magmas ascended through the same fracture network, leading to commingling of the magmas at, or near, their sites of final crystallisation. Widespread propylitic alteration (30) was the final manifestation of magmatic–hydrothermal activity at Northparkes.

monzonitic magmas. Given the intrusive contact relationships, it is envisaged that the two magmas ascended mainly through the same fracture network, which led to the commingling of the basaltic trachyandesitic and monzonitic magmas at, or close to the site of their solidification.

CONCLUSIONS

The Goonumbla and Wombin Volcanics and related intrusions, including the BQM intrusions, show a coherent trend from basaltic trachyandesite through to trachyte, with increasing K_2O and decreasing TiO_2, Al_2O_3, Fe_2O_3, CaO and MgO contents with increasing SiO_2 contents. These trends continue through to the evolved quartz monzonite porphyry intrusions associated with the Northparkes deposits. The consistent overlap and similar character of trends in most of the major and trace elements with respect to SiO_2, MgO and TiO_2 indicate the broadly comagmatic nature of these intrusive and volcanic rocks. The spike-patterned multi-element plots are typical of magmas generated in subduction-related tectonic settings. This subduction-related setting is supported by the pronounced Fe-depletion with increasing SiO_2.

The sequence of intrusion of the various phases in the quartz monzonite porphyry complexes at Northparkes is different from that of many other porphyry Cu districts, such as the Laramide magmatic complexes of Arizona, where there is a distinct evolution in the intrusive phases from less to more felsic with time (Lang & Titley 1998). In contrast, although intrusive phases associated with the Northparkes deposits initially evolve to more felsic compositions, later intrusive events were significantly less felsic, suggesting that magmatic fractionation alone cannot account for the intrusive history at Northparkes. Our preferred genetic model therefore centres on the emplacement of a series of mafic alkaline melts into the base of a crystallising, zoned monzodiorite to monzonite magma chamber at Northparkes.

Besides being intimately associated with K-silicate alteration assemblages and Cu–Au mineralisation, there are several differences between the mineralised quartz monzonite porphyry complexes at Northparkes and unmineralised intrusions elsewhere in the district that may be of interest to future exploration: (i) the mineralised intrusions contain up to 10% quartz and are distinctly more fractionated than any of the intrusions related to the Goonumbla or Wombin volcanics; (ii) the unidirectional solidification textures and miarolitic cavities that are abundant in the K-QMP, and are present in the KA-QMP intrusions (Lickfold *et al.* 2003), do not occur in the other intrusions of the Northparkes district; (iii) the mineralised quartz monzonite porphyries are enriched in K, Ba and Sr, and depleted in Rb, Nb and Zr compared to the BQM and regional intrusions; (iv) B-QMP, KA-QMP and K-QMP intrusions show increasing LREE depletion compared to the regional intrusions; and (v) basaltic trachyandesite dykes are commingled with mafic monzonite porphyry intrusions at E26, a feature not recognised elsewhere in the Northparkes district.

Downloaded by [Ondokuz Mayis Universitesine] at 17:04 13 November 2014

ACKNOWLEDGEMENTS

We thank Northparkes Mines and North Ltd for logistical and financial support during the PhD study of the Northparkes Cu–Au deposits and for giving us permission to publish this paper. In particular, Bob Beeson, Mark Arundell and Stuart Smith are thanked for their assistance throughout the conception and implementation of this research project. Phil Robinson and Mark Norman are thanked for conducting XRF and REE analyses at the University of Tasmania. Carol Simpson provided additional regional rock samples and thin-sections. June Pongratz assisted in figure preparation. VL received PhD scholarship and research funding from the University of Tasmania and North Ltd. Funding from the Australian Research Council through their Special Research Centre and Centre of Excellence programs is also gratefully acknowledged. We thank Anthony Harris and John Walshe for their thorough reviews of this manuscript, and Dick Glen for his editorial comments.

REFERENCES

ANDERS R. J., ROSE W. I., KYLE P. R., DESILVA S., FRANCIS P., GARDEWEG M. & MORENO R. H. 1991. Excessive sulfur dioxide emissions from Chilean volcanoes. *Journal of Volcanology and Geothermal Research* **46**, 323–329.

ARUNDELL M. C. 1997. Goonumbla: 25 years, four deposits, 52 prospects and still drilling. *In*: *3rd International Mining Geology Conference Proceedings*, pp. 183–187. Australasian Institute of Mining and Metallurgy, Melbourne.

ARUNDELL M. C. 1998. The geology and mineralisation of the E31 copper–gold prospect, Goonumbla, N.S.W. MEconGeol. thesis, University of Tasmania, Hobart (unpubl.).

BALDWIN J. A. & PEARCE J. A. 1982. Discrimination of productive and non-productive porphyritic intrusions in the Chilean Andes. *Economic Geology* **77**, 664–674.

BEA F. 1996. Residence of REE, Y, Th and U in granites and crustal protoliths; implications for the chemistry of crustal melts. *Journal of Petrology* **37**, 521–552.

BLEVIN P. L. & MORRISON G. W. 1997. Magmatic and hydrothermal evolution of major intrusive related gold deposits. AMIRA P425, Final Report, Parts 11 & 14 (unpubl.).

BOWMAN H. N., RICHARDSON S. J. & DOLANSKI J. 1982. *Narromine 1:250 000 Metallogenic Map SI 55–3 Mine Data Sheets and Metallogenic Study*. New South Wales Geological Survey, Sydney.

BUTERA K. M., WILLIAMS I. S., BLEVIN P. L. & SIMPSON C. J. 2001. Zircon U–Pb dating of Early Palaeozoic monzonitic intrusives from the Goonumbla area, New South Wales. *Australian Journal of Earth Sciences* **48**, 457–464.

CANDELA P. A. 1984. A partitioning model for the rare earth elements and other polyvalent, chloride-complexed metals in melt–vapor systems. *Geological Society of America Abstracts with Programs* **16**, 462.

CANDELA P. A. 1990. Theoretical constraints on the chemistry of the magmatic aqueous phase. *In*: Stein H. J. & Hannah J. L. eds. *Ore-bearing Granite Systems: Petrogenesis and Mineralizing Processes*, pp. 11–20. Geological Society of America Special Paper **246**.

CARTEN R. B., WALKER B. M. & GERAGHTY E. P. 1988. Comparison of field-based studies of the Henderson porphyry molybdenum deposit, Colorado, with experimental and theoretical models of porphyry systems. *In*: Taylor R. P. & Strong D. F. eds. *Recent Advances in the Geology of Granite-related Mineral Deposits*, pp. 351–366. Canadian Institute of Mining and Metallurgy Special Volume **39**.

CLARKE I. 1990. Igneous petrology. *In*: Clarke I. and Sherwin L. eds. *Geological Setting of Gold and Copper Deposits in the Parkes Area, New South Wales*, pp. 95–136. Records of the Geological Survey of New South Wales **23**.

Downloaded by [Ondokuz Mayis Universitesine] at 17:04 13 November 2014

COLE J. W., GAMBLE J. A., BURT R. M., CARROLL L D. & SHELLEY D. 2001. Mixing and mingling of andesite–dacite magmas: evidence from co-magmatic plutonic enclaves, Taupo Volcanic Zone, New Zealand. *Lithos* **59**, 25–46.

COOKE D. R., WILSON A. J., HOUSE M. J., WOLFE R. C., WALSHE J. L., LICKFOLD V. & CRAWFORD A. J. 2007. Alkalic porphyry Au–Cu and associated mineral deposits of the Ordovician to Early Silurian Macquarie Arc, New South Wales. *Australian Journal of Earth Sciences* **54**, 445–463.

COOMBS M. L., EICHELBERGER J. C. & RUTHERFORD M. J. 2000. Magma storage and mixing conditions for the 1953–1974 eruptions of Southwest Trident Volcano, Katmai National Park, Alaska. *Contributions to Mineralogy and Petrology* **140**, 99–118.

CRAWFORD A. J. 2001. Lithostratigraphy and lithochemistry of volcanic and intrusive rocks, Parkes–Narromine belt. *In*: Crawford A. J., Cooke D. R. & Glen R. A. eds. *NSW Ordovician SPIRT Report*, pp. 2.19–2.41. Centre for Ore Deposit Research, University of Tasmania, Hobart (unpubl.).

CRAWFORD A. J., COOKE D. R. & GLEN R. A. 2001. NSW Ordovician SPIRT Report. Centre for Ore Deposit Research, University of Tasmania, Hobart (unpubl.).

CRAWFORD A. J., MEFFRE S., SQUIRE R. J., BARRON L. M. & FALLOON T. J. 2007. Middle and Late Ordovician magmatic evolution of the Macquarie Arc, Lachlan Orogen, New South Wales. *Australian Journal of Earth Sciences* **54**, 181–214.

DE HOOG J. C. M. & VAN BERGEN M. J. 2000. Volatile-induced transport of HSFE, REE, Th and U in arc magma: evidence from zirconolite-bearing vesicles in potassic lavas of Lewotolo volcano (Indonesia). *Contributions to Mineralogy and Petrology* **139**, 485–502.

DUGGAN M. B., LYONS P., RAYMOND O. L., WALLACE D. A., WYBORN D., YOUNG G. C., KRYNEN J. P., SCOTT M. M. & SHERWIN L. 1999. *Forbes 1:250 000 Geological Map S155–7* (Preliminary edition). Australian Geological Survey Organisation, Canberra and Geological Survey of New South Wales, Sydney.

FOURNELLE J. 1990. Anhydrite in Nevada del Ruiz November 1985 pumice: relevance to the sulfur problem. *Journal of Volcanology and Geothermal Research* **42**, 189–201.

GILL J. B. 1981. *Orogenic Andesites and Plate Tectonics*. Springer, Berlin.

GLEN R. A., CRAWFORD A. J., PERCIVAL I. G. & BARRON L. M. 2007. Early Ordovician development of the Macquarie Arc, Lachlan Orogen, New South Wales. *Australian Journal of Earth Sciences* **54**, 167–179.

GLEN R. A. & WALSHE J. L. 1999. Cross-structures in the Lachlan Orogen: the Lachlan Transverse Zone example. *Australian Journal of Earth Sciences* **46**, 641–658.

GLEN R. A., WALSHE J. L., BARRON L. M. & WATKINS J. J. 1998. Ordovician convergent-margin volcanism and tectonism in the Lachlan sector of east Gondwana. *Geology* **26**, 751–754.

GREEN T. H. 1980. Island arc and continent-building magmatism; a review of petrogenic models based on experimental petrology and geochemistry. *Tectonophysics* **63**, 367–385.

GUSTAFSON L. B. & HUNT J. P. 1975. The porphyry copper deposit at El Salvador, Chile. *Economic Geology* **70**, 857–912.

HALL M. C. 1993. The stratigraphy and palaeovolcanology of the Late Ordovician Goonumbla Volcanic Complex, Goonumbla, N.S.W. BSc (Hons) thesis, Monash University, Melbourne (unpubl.).

HALTER W. E., HEINRICH C. A. & PETTKE T. 2005. Magma evolution and the formation of porphyry Cu–Au ore fluids: evidence from silicate and sulfide melt inclusions. *Mineralium Deposita* **39**, 845–863.

HARRIS A. C. 1997. Vein emplacement, E26N porphyry Cu–Au deposit, Goonumbla, New South Wales. BSc (Hons) thesis, University of Queensland, Brisbane (unpubl.).

HARRIS A. C. & GOLDING S. D. 2002. New evidence of magmatic-fluid-related phyllic alteration: implications for the genesis of porphyry Cu deposits. *Geology* **30**, 335–338.

HASSANEN M. A. 1997. Post-collision, A-type granites of Homrit Wagga Complex, Egypt: petrological and geochemical constraints on its origin. *Precambrian Research* **82**, 211–236.

HATTORI K. H. & KEITH J. D. 2001. Contribution of mafic melt to porphyry copper mineralization: evidence from Mount Pinatubo, Philippines and Bingham deposit, Utah. *Mineralium Deposita* **36**, 799–806.

HEITHERSAY P. S. 1991. The shoshonite-associated Endeavour 26 North porphyry copper–gold deposit, Goonumbla, NSW. PhD thesis, Australian National University, Canberra (unpubl.).

HEITHERSAY P. S. 1994. The central west New South Wales Cu–Au province: porphyry copper–gold deposits. CODES, University of Tasmania, Master of Economic Geology Short-Course Manual **1** (unpubl.).

HEITHERSAY P. S., O'NEILL W. J., VAN DER HELDER P., MOORE C. R. & HARBON P. G. 1990. Goonumbla porphyry copper district—Endeavour 26 North, Endeavour 22 and Endeavour 27 copper–gold deposits. *In*: Hughes F. E. ed. *Geology of the Mineral Deposits of Australia and Papua New Guinea*, pp. 1385–1398. Australasian Institute of Mining and Metallurgy Monograph **14**.

HEITHERSAY P. S. & WALSHE J. L. 1995. Endeavour 26 North: a porphyry copper–gold deposit in the Late Ordovician shoshonitic Goonumbla Volcanic Complex, New South Wales, Australia. *Economic Geology* **90**, 1506–1532.

HOLLIDAY J. R., WILSON A. J., BLEVIN P. L., TEDDER I. J., DUNHAM P. D. & PFITZNER M. 2002. Porphyry gold–copper mineralisation in the Cadia district, eastern Lachlan Fold Belt, New South Wales, and its relationship to shoshonitic magmatism. *Mineralium Deposita* **37**, 100–116.

HOOPER B., HEITHERSAY P. S., MILLS M. B., LINDHORST J. W. & FREYBERG J. 1996. Shoshonite-hosted Endeavour 48 porphyry copper–gold deposit, Northparkes, central New South Wales. *Australian Journal of Earth Sciences* **43**, 179–288.

HOUSE M. J. 1994. Gold distribution at the E26 porphyry copper–gold deposit, N.S.W. MEconGeol thesis, University of Tasmania, Hobart (unpubl.).

HOWLAND-ROSE J. S. 1996. Fluid evolution at the Endeavour 48 porphyry Cu–Au deposit, Parkes, NSW. BSc (Hons) thesis, University of Newcastle, Newcastle (unpubl.).

JENSEN E. P. & BARTON M. D. 2000. Gold deposits related to alkaline magmatism. *Reviews in Economic Geology* **13**, 279–314.

JONES G. J. 1985. The Goonumbla porphyry copper deposits, New South Wales. *Economic Geology* **80**, 591–613.

KAZAHAYA K., SHINOHARA H. & SAITO G. 1994. Excessive degassing of Izu-Oshima volcano: magma convection in a conduit. *Bulletin of Volcanology* **56**, 207–216.

KEITH J. D., CHRISTIANSEN E. H. & CARTEN R. B. 1993. The genesis of giant porphyry molybdenum deposits. *In*: Whiting B. H., Mason R. & Hodgson C. J. eds. *Giant Ore Deposits*, pp. 285–317. Society of Economic Geologists Special Publication **2**.

KEITH J. D., CHRISTIANSEN E. H., MAUGHAN D. T. & WAITE K. A. 1998. The role of mafic alkaline magmas in felsic porphyry Cu and Mo systems. *In*: Lentz D. R. ed. *Mineralized Intrusion-related Skarn Systems*, pp. 211–243. Mineralogical Association of Canada Short Course Series **26**.

KEITH J. D., WHITNEY J. A., HATTORI K., BALLANTYNE G. H., CHRISTIANSEN E. H., BARR D. L., CANNAN T. M. & HOOK C. J. 1997. The role of magmatic sulfides and mafic alkaline magmas in the Bingham and Tintic mining districts, Utah. *Journal of Petrology* **38**, 1679–1690.

KIRKHAM R. V. & SINCLAIR W. D. 1988. Comb quartz layers in felsic intrusions and their relationship to porphyry deposits. *In*: Taylor R. P. & Strong D. F. eds. *Recent Advances in the Geology of Granite-related Mineral Deposits*, pp. 50–71. Canadian Institute of Mining and Metallurgy Special Volume **39**.

KOLKERT R. 1998. Carbonate–base metal veins peripheral to the Goonumbla Cu–Au deposits—vectors to mineralized centres BSc (Hons) thesis, University of Tasmania, Hobart (unpubl.).

KRESS V. 1997. Magma mixing as a source for Pinatubo sulfur. *Nature* **389**, 591–593.

KRYNEN J. P., SHERWIN L. & CLARKE I. 1990. Stratigraphy and structure. *In*: Clarke I. & Sherwin L. eds. *Geological Setting of Gold and Copper Mineralisation in the Parkes area, New South Wales*, pp. 1–76. Records of the Geological Survey of New South Wales **23**.

LANG J. R. & TITLEY S. R. 1998. Isotopic and geochemical characteristics of Laramide magmatic systems in Arizona and implication for the genesis of porphyry copper deposits. *Economic Geology* **93**, 138–170.

LE BAS M. J., LE MAITRE R. W., STRECKEISEN A. & ZANETTIN B. 1986. A chemical classification of volcanic rocks based on the total alkali–silica diagram. *Journal of Petrology* **27**, 745–750.

LICKFOLD V. 2002. Intrusive history and volatile evolution of the Endeavour porphyry Cu–Au deposits, Goonumbla district, NSW, Australia. PhD thesis, University of Tasmania, Hobart (unpubl.).

LICKFOLD V., COOKE D. R., SMITH S. G. & ULLRICH T. 2003. Endeavour Cu–Au porphyry deposits, Northparkes, NSW—intrusive history and fluid evolution. *Economic Geology* **98**, 1607–1636.

LUDWIG K. R. 2001. SQUID 1.02, A User's Manual. *Berkeley Geochronology Center Special Publication* **2**.

LUDWIG K. R. 2003. User's manual for Isoplot/Ex, Version 3.0, a geochronological toolkit for Microsoft Excel. *Berkeley Geochronology Center Special Publication* **4**.

LYE A., CROOK G. & KOLFF VAN OOSTERWIJK L. 2006. The discovery history of the Northparkes deposits. *In*: Lewis P. C. ed. *Mineral Exploration Geoscience in New South Wales*, pp. 21–25. SMEDG Mines and Wines Conference, Cessnock NSW, Extended Abstracts.

MACDONALD G. D. & ARNOLD L. C. 1994. Geological and geochemical zoning of the Grasberg Igneous Complex, Irian Jaya, Indonesia. *In*: van Leeuwen T. M., Hedenquist J. W., James L. P. & Dow J. A. S. eds. *Mineral Deposits in Indonesia: Discoveries of the Past 25 Years*, pp. 143–178. Journal of Geochemical Exploration **50**.

MAUGHAN D. T., KEITH J. D., CHRISTIANSEN E. H., PULSIPHER T., HATTORI K. & EVANS N. J. 2002. Contributions from mafic alkaline magmas to the Bingham porphyry Cu–Au–Mo deposit, Utah, USA. *Mineralium Deposita* **37**, 14–37.

MCKAY G. A. 1989. Partitioning of rare earth elements between major silicate minerals and basaltic melts. *In*: Lipin B. R. & McKay G. A. eds. *Geochemistry and Mineralogy of Rare Earth Elements*, pp. 45–77. Reviews in Mineralogy **21**.

MÜLLER D., HEITHERSAY P. S. & GROVES D. I. 1994. The shoshonite porphyry Cu–Au association in the Goonumbla district, N.S.W., Australia. *Mineralogy and Petrology* **51**, 299–321.

NORTH LTD 1999. Structural evolution and controls on Cu–Au mineralisation, Goonumbla Region, Confidential Company Report.

PACES J. B. & MILLER J. D. 1993. Precise U–Pb ages of Duluth Complex and related mafic intrusions, northeastern Minnesota: geochronological insights to physical, petrogenetic, paleomagnetic, and tectonomagmatic process associated with the 1.1 Ga Midcontinent Rift System. *Journal of Geophysical Research* **98**, 13997–14013.

PALLISTER J. S., HOBLITT R. P., MEEKER G. P., KNIGHT R. J. & SIEMS D. F. 1996. Magma mixing at Mount Pinatubo: petrographic and chemical evidence from the 1991 deposits. *In*: Newhall C. G. & Punongbayan R. S. eds. *Fire and Mud: Eruptions and Lahars of Mount Pinatubo*, pp. 687–731. PHIVOLCS and University of Washington Press, Seattle.

PASTERIS J. D. 1996. Mount Pinatubo volcano and 'negative' porphyry copper deposits. *Geology* **24**, 1075–1078.

PECCERILLO A. & TAYLOR S. R. 1976. Geochemistry of Eocene calc-alkaline volcanic rocks from the Kastamonu area, northern Turkey. *Contributions to Mineralogy and Petrology* **58**, 63–81.

PERCIVAL I. G. 2000. Northparkes Volcanic Group. *In*: Lyons P., Raymond O. L. & Duggan M. B. eds. *Forbes 1:250 000 Geological Sheet SI/55–7, 2nd edition, Explanatory Notes*, pp. 19–21. Australian Geological Survey Organisation Record **2000/20**.

PERCIVAL I. G. & GLEN R. A. 2007. Ordovician to earliest Silurian history of the Macquarie Arc, Lachlan Orogen, New South Wales. *Australian Journal of Earth Sciences* **54**, 143–165.

PERKINS C., MCDOUGALL I. & CLAOUÉ-LONG J. 1990. $^{40}Ar/^{39}Ar$ and U–Pb geochronology of the Goonumbla porphyry Cu–Au deposits, New South Wales, Australia. *Economic Geology* **85**, 1808–1824.

POLLARD P. J. & TAYLOR R. G. 2002. Paragenesis of the Grasberg Cu–Au deposit, Irian Jaya, Indonesia: results from logging section 13. *Mineralium Deposita* **37**, 117–136.

PROFFETT J. M. 2003. Geology of the Bajo de la Alumbrera porphyry copper–gold deposit, Argentina. *Economic Geology* **98**, 1535–1574.

RADCLYFFE D. 1995. Regional-scale propylitic alteration in the Goonumbla mineral field, Parkes, NSW. BSc (Hons) thesis, University of Tasmania, Hobart (unpubl.).

RICHARDS J. P. 1997. Controls on scale of Porgera-type porphyry/epithermal gold deposits associated with mafic, alkalic magmatism. *Transactions of the Institution of Mining and Metallurgy* **106**, B1–B8.

ROWLAND M. G. & WILKINSON J. J. 1999. Significance of intermediate stage veins at Quebrada Blanca, Chile. *In*: Stanley C. J. *et al.* eds. *Mineral Deposits: Processes to Processing*, pp. 99–102. A. A. Balkema, Rotterdam.

SAMBRIDGE M. S. & COMPSTON W. 1994. Mixture modelling of multi-component data sets with application to ion-probe zircon ages. *Earth and Planetary Science Letters* **128**, 373–390.

SCHEIBNER E. & BASDEN H. (EDITORS) 1998. Geology of New South Wales—Synthesis. Volume 2 Geological Evolution. *Geological Survey of New South Wales Memoir* **13(2)**.

SCOTT K. M. 2005. Rutile geochemistry as a guide to porphyry Cu–Au mineralization, Northparkes, New South Wales, Australia. *Geochemistry: Exploration, Environment, Analysis* **5**, 247–253.

SEEDORFF E. & EINAUDI M. T. 2004. Henderson porphyry molybdenum system, Colorado: II. Decoupling of introduction and deposition of metals during geochemical evolution of hydrothermal fluids. *Economic Geology* **99**, 3–37.

SHERWIN L. 1996. *Narromine 1:250 000 Geological Sheet SI/55–3, Explanatory Notes.* Geological Survey of New South Wales, Sydney.

SHINOHARA H., KAZAHAYA K. & LOWENSTERN J. B. 1995. Volatile transport in a convecting magma column: implications for porphyry Mo mineralisation. *Geology* **23**, 1091–1094.

SILLITOE R. H. 1997. Characteristics and controls of the largest porphyry copper–gold and epithermal gold deposits in the circum-Pacific region. *Australian Journal of Earth Sciences* **44**, 373–388.

SILLITOE R. H. 2000. Gold-rich porphyry deposits: descriptive and genetic models and their role in exploration and discovery. *Society of Economic Geologists Reviews* **13**, 315–345.

SILLITOE R. H. & GAPPE I. M. J. 1984. Philippine porphyry copper deposits: geologic setting and characteristics. United Nations Development Program, Technical support for regional offshore prospecting in East Asia, CCOP/TP14, RAS/81/120.

SIMPSON C. J., CAS R. A. F. & ARUNDELL M. C. 2005. Volcanic evolution of a long-lived Ordovician island-arc province in the Parkes region of the Lachlan Fold Belt, southeastern Australia. *Australian Journal of Earth Sciences* **52**, 863–886.

SMITH D. R., NOBLETT J., WOBUS R. A., UNRUH D. M., DOUGLASS J., BEANE R., DAVIS C., GOLDMAN S., KAY G., GUSTAVSON B., SALTOUN B. & STEWART J. 1999. Petrology and geochemistry of late-stage intrusions of the A-type, mid-Proterozoic Pikes Peak Batholith (central Colorado, USA): implications for petrogenetic models. *Precambrian Research* **98**, 271–305.

SQUIRES V. E. 1992. The mineralisation and alteration of the Endeavour 27 porphyry copper–gold deposit, Goonumbla, New South Wales. BSc (Hons) thesis, University of Sydney (unpubl.).

SUN S-S. & MCDONOUGH W. F. 1989. Chemical and isotopic systematics of oceanic basalts; implications for mantle composition and processes. *In*: Saunders A. D. & Norry M. J. eds. *Magmatism in the Ocean Basins*, pp. 313–345. Geological Society of London Special Publication **42**.

TERA F. & WASSERBURG G. 1972. U–Th–Pb systematics in three Apollo 14 basalts and the problem of initial Pb in lunar rocks. *Earth and Planetary Science Letters* **14**, 281–304.

WEBSTER J. D., HOLLOWAY J. R. & HERVIG R. L. 1989. Partitioning of lithophile trace elements between H_2O and $H_2O–CO_2$ fluids and topaz rhyolite melt. *Economic Geology* **84**, 116–134.

WILLIAMS I. S. 1998. U–Th–Pb geochronology by ion microprobe. *In*: McKibben M. A., Shanks W. C. III & Ridley W. I. eds. *Applications of Microanalytical Techniques to Understanding Mineralizing Processes*, pp. 1–35. Reviews in Economic Geology **7**.

WILSON A. J., COOKE D. R. & HARPER B. L. 2003. The Ridgeway gold–copper deposit: a high-grade alkalic porphyry deposit in the Lachlan Fold Belt, New South Wales, Australia. *Economic Geology* **98**, 1637–1666.

WILSON A. J., COOKE D. R., HARPER B. J. & DEYELL C. L. Sulfur isotopic zonation in the Cadia district, southeastern Australia: exploration significance and implications for the genesis of alkalic porphyry gold–copper deposits. *Mineralium Deposita* (in press). Online http://www.springerlink.com/content/b2jp14782129jg78/?.p=3ada3af82d574fca93f2d6ff4fee4a64&pi=1.

WOLFE R. C. 1994. The geology, paragenesis and alteration geochemistry of the Endeavour 48 Cu–Au porphyry, Goonumbla N.S.W. BSc (Hons) thesis, University of Tasmania, Hobart (unpubl.).

WOLFE R. C., COOKE D. R., HOOPER B. & HEITHERSAY P. S. 1996. A magmatic origin for late-stage sericite–alunite alteration at the Endeavour 48 Cu–Au porphyry deposit, Goonumbla, NSW. *Geological Society of Australia Abstracts* **41**, 480.

Received 7 March 2004; accepted 31 October 2006

Downloaded by [Ondokuz Mayis Universitesine] at 17:04 13 November 2014

Downloaded by [Ondokuz Mayis Universitesine] at 17:04 13 November 2014

APPENDIX 1: ANALYTICAL PROCEDURE FOR U–PB GEOCHRONOLOGY

Zircon grains were separated from total rock samples using standard crushing, washing, heavy-liquid (SG 2.96 and 3.3) and paramagnetic procedures. Hand-selected zircon grains were placed onto double-sided tape, mounted in epoxy together with chips of the reference zircons (FC1 and SL13), sectioned approximately in half and polished. Reflected and transmitted light photomicrographs were prepared for all zircons, as were cathodoluminescence scanning electron microscope images. The cathodoluminescence images were used to decipher the internal structures of the sectioned grains and to ensure that the $\sim$20 μm SHRIMP spot was wholly within a single age component in the sectioned grains.

The U–Th–Pb analyses were made using SHRIMP II at the Research School of Earth Sciences, Australian National University, Canberra, following procedures given in Williams (1998 and references therein). Each analysis consisted of six scans through the mass range, with the FC1 U–Pb reference grains analysed for every three unknown analyses. The data have been reduced using the SQUID Excel Macro of Ludwig (2001). The Pb/U ratios have been normalised relative to a value of 0.1859 for the $^{206}Pb/^{238}U$ ratio of the FC1 reference zircons, equivalent to an age of 1099 Ma (Paces & Miller 1993).

Uncertainties given for individual analyses (ratios and ages) are at the 1σ level (Tables 3, 4). Tera and Wasserburg (1972) concordia plots, probability density plots with stacked histograms and weighted mean $^{206}Pb/^{238}U$ age calculations were carried out using ISOPLOT/EX (Ludwig 2003). The mixture modelling algorithm of Sambridge and Compston (1994), via ISOPLOT/EX, was used to unmix statistical age populations or groupings; from these groups, weighted mean $^{206}Pb/^{238}U$ ages were assessed and the preferred crystallisation ages calculated with uncertainties reported as 95% confidence limits.

The results are summarised in Tables 3 and 4.

Table 3 Summary of SHRIMP U–Pb results for zircon from the E26 biotite quartz monzonite (E26 DDH287, 220.6 m).

Grain. spot	U (ppm)	Th (ppm)	Th/U	$^{206}Pb^*$ (ppm)	$^{204}Pb/^{206}Pb$	f_{206} %	Total radiogenic age (Ma)							
							$^{238}U/^{206}Pb$	±	$^{207}Pb/^{206}Pb$	±	$^{206}Pb/^{238}U$	±	$^{206}Pb/^{238}U$	±
1.1	230	167	0.73	14.2	0.000110	0.12	13.890	0.156	0.0569	0.0007	0.0719	0.0008	447.6	4.9
2.1	602	500	0.83	37.6	0.000026	<0.01	13.778	0.145	0.0555	0.0004	0.0726	0.0008	452.0	4.7
3.1	243	169	0.70	15.1	0.000141	0.09	13.790	0.157	0.0567	0.0006	0.0725	0.0008	450.9	5.0
4.1	360	276	0.77	21.9	0.000050	0.03	14.151	0.153	0.0559	0.0005	0.0706	0.0008	440.0	4.7
5.1	298	216	0.73	18.1	0.000098	0.03	14.157	0.156	0.0560	0.0006	0.0706	0.0008	439.8	4.8
6.1	285	169	0.59	17.5	–	0.14	13.980	0.154	0.0569	0.0006	0.0714	0.0008	444.8	4.8
7.1	195	137	0.70	12.3	0.000030	0.02	13.615	0.155	0.0563	0.0007	0.0734	0.0009	456.8	5.1
8.1	388	325	0.84	23.8	–	0.04	13.987	0.150	0.0561	0.0005	0.0715	0.0008	445.0	4.7
9.1	671	773	1.15	41.5	–	0.02	13.887	0.145	0.0561	0.0004	0.0720	0.0008	448.2	4.6
10.1	561	444	0.79	35.0	0.000060	<0.01	13.761	0.155	0.0550	0.0004	0.0728	0.0008	452.8	5.0
11.1	682	497	0.73	41.3	0.000065	0.12	14.189	0.149	0.0567	0.0004	0.0704	0.0008	438.5	4.5
12.1	364	296	0.81	22.7	0.000166	<0.01	13.756	0.149	0.0558	0.0005	0.0727	0.0008	452.5	4.8
13.1	414	317	0.77	24.6	0.000019	0.15	14.431	0.154	0.0567	0.0005	0.0692	0.0007	431.3	4.5
14.1	353	300	0.85	21.3	0.000024	0.14	14.240	0.153	0.0567	0.0005	0.0701	0.0008	436.9	4.6
15.1	646	562	0.87	39.2	0.000002	0.01	14.144	0.148	0.0558	0.0004	0.0707	0.0007	440.3	4.5
16.1	101	54	0.53	6.4	0.000079	<0.01	13.661	0.201	0.0546	0.0009	0.0733	0.0011	456.2	6.6
17.1	267	208	0.78	16.1	0.000179	0.09	14.213	0.157	0.0563	0.0006	0.0703	0.0008	438.0	4.7
18.1	614	513	0.84	37.4	0.000003	0.09	14.091	0.148	0.0564	0.0004	0.0709	0.0008	441.6	4.5
19.1	380	336	0.88	24.0	–	0.04	13.630	0.148	0.0565	0.0005	0.0733	0.0008	456.2	4.9
20.1	198	93	0.47	12.0	0.000050	0.06	14.138	0.162	0.0562	0.0007	0.0707	0.0008	440.3	5.0
											Weighted mean		**444.2**	**4.7**

Uncertainties given at the 1σ level.
Error in FC1 reference zircon calibration was 0.81% for the analytical session (not included in the above errors but required when comparing data from different mounts).
f_{206} % denotes the percentage of ^{206}Pb that is common Pb.
Correction for common Pb made using the measured $^{238}U/^{206}Pb$ and $^{207}Pb/^{206}Pb$ ratios following Tera and Wasserburg (1972) as outlined in Williams (1998).

Table 4 Summary of SHRIMP U–Pb results for zircon from the E37 zero porphyry: (E37 DDH3, 245.2 m).

Grain. spot	U (ppm)	Th (ppm)	Th/U	$^{206}Pb^*$ (ppm)	$^{204}Pb/^{206}Pb$	f_{206} %	Total radiogenic age (Ma)							
							$^{238}U/^{206}Pb$	±	$^{207}Pb/^{206}Pb$	±	$^{206}Pb/^{238}U$	±	$^{206}Pb/^{238}U$	±
1.1	503	452	0.90	28.9	0.000036	0.28	14.943	0.168	0.0574	0.0006	0.0667	0.0008	416.4	4.6
2.1	699	784	1.12	42.1	0.000038	0.12	14.288	0.149	0.0565	0.0005	0.0699	0.0007	435.6	4.5
3.1	109	61	0.56	6.5	0.000241	0.90	14.449	0.181	0.0626	0.0010	0.0686	0.0009	427.6	5.3
4.1	504	542	1.08	30.3	0.000253	0.45	14.302	0.160	0.0592	0.0004	0.0696	0.0008	433.8	4.8
5.1	96	37	0.39	5.8	–	0.70	14.178	0.185	0.0613	0.0010	0.0700	0.0009	436.4	5.6
6.1	298	260	0.87	18.6	0.000100	0.14	13.740	0.153	0.0571	0.0005	0.0727	0.0008	452.3	4.9
7.1	192	137	0.71	11.6	0.000069	0.34	14.288	0.162	0.0583	0.0007	0.0697	0.0008	434.6	4.8
8.1	149	84	0.57	9.1	–	0.40	14.071	0.163	0.0589	0.0008	0.0708	0.0008	440.9	5.0
9.1	452	403	0.89	26.9	0.000055	0.22	14.423	0.153	0.0573	0.0004	0.0692	0.0007	431.2	4.5
10.1	312	198	0.64	19.2	0.000107	0.07	13.956	0.151	0.0564	0.0005	0.0716	0.0008	445.8	4.7
11.1	349	324	0.93	20.7	–	0.33	14.520	0.159	0.0581	0.0005	0.0686	0.0008	428.0	4.6
12.1	152	97	0.64	9.4	0.000794	0.92	13.878	0.160	0.0633	0.0016	0.0714	0.0008	444.5	5.1
13.1	169	79	0.47	10.5	0.000242	0.28	13.848	0.160	0.0582	0.0007	0.0720	0.0008	448.3	5.1
14.1	152	82	0.54	9.2	0.000405	0.74	14.200	0.193	0.0615	0.0013	0.0699	0.0010	435.6	5.8
15.1	118	56	0.48	7.2	0.000303	0.72	14.206	0.178	0.0614	0.0009	0.0699	0.0009	435.5	5.4
16.1	259	124	0.48	16.1	0.000161	0.03	13.837	0.154	0.0562	0.0006	0.0722	0.0008	449.7	4.9
17.1	260	146	0.56	15.8	0.000128	0.25	14.152	0.157	0.0577	0.0006	0.0705	0.0008	439.1	4.8
18.1	393	298	0.76	23.9	0.000009	0.10	14.112	0.151	0.0565	0.0005	0.0708	0.0008	440.9	4.6
19.1	431	396	0.92	25.8	0.000036	0.14	14.337	0.153	0.0566	0.0005	0.0697	0.0008	434.1	4.5
20.1	234	145	0.62	14.0	0.000054	0.35	14.335	0.160	0.0584	0.0006	0.0695	0.0008	433.2	4.7
											Weighted mean		**436.7**	**3.3**

Uncertainties given at the 1σ level.
Error in FC1 reference zircon calibration was 0.32% for the analytical session (not included in the above errors but required when comparing data from different mounts).
f_{206} % denotes the percentage of ^{206}Pb that is common Pb.
Correction for common Pb made using the measured $^{238}U/^{206}Pb$ and $^{207}Pb/^{206}Pb$ ratios following Tera and Wasserburg (1972) as outlined in Williams (1998).

Downloaded by [Ondokuz Mayis Universitesine] at 17:04 13 November 2014